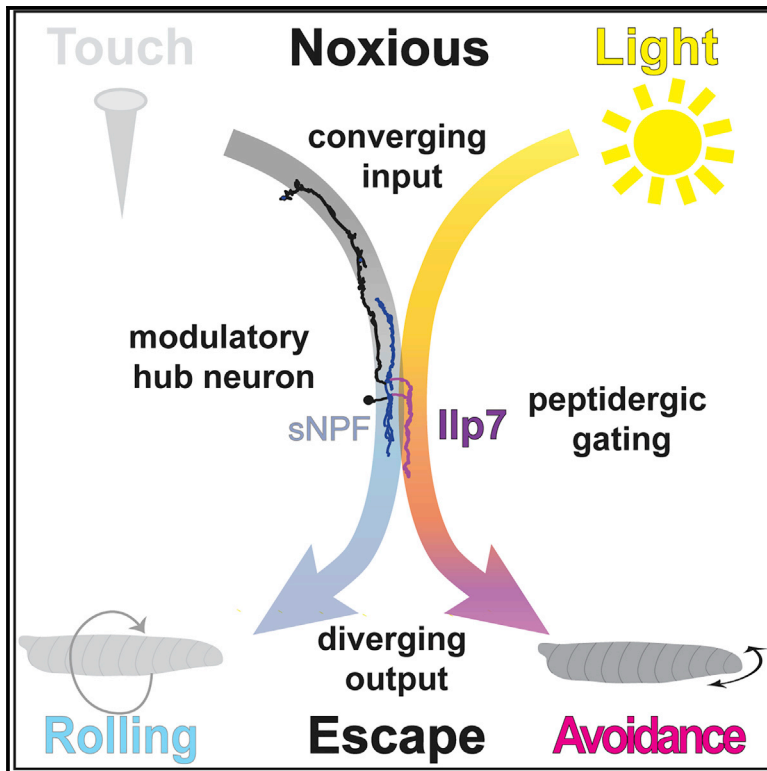


Current Biology

A neuropeptidergic circuit gates selective escape behavior of *Drosophila* larvae

Graphical abstract



Authors

Bibi Nusreen Imambocus, Fangmin Zhou, Andrey Formozov, ..., Alisson M. Gontijo, Albert Cardona, Peter Soba

Correspondence

psoba@uni-bonn.de

In brief

Animals escape from danger using stimulus-specific responses. Imambocus et al. show that in *Drosophila* larvae, neuromodulatory hub neurons help to discriminate noxious stimuli and facilitate specific behavioral responses by acute neuropeptide release to promote avoidance of noxious light.

Highlights

- Connectome of a neuromodulatory circuit required for noxious light avoidance
- Domain-specific input of noxious light and touch circuits on modulatory hub neurons
- Acute neuropeptide release from hub neurons gates noxious light avoidance
- Noxious light and touch are differentiated by selective peptide-responsive circuits

Article

A neuropeptidergic circuit gates selective escape behavior of *Drosophila* larvae

Bibi Nusreen Imambocus,^{1,2} Fangmin Zhou,^{1,2} Andrey Formozov,² Annika Wittich,² Federico M. Tenedini,² Chun Hu,^{2,11} Kathrin Sauter,² Ednilson Macarenhas Varela,³ Fabiana Herédia,³ Andreia P. Casimiro,³ André Macedo,³ Philipp Schlegel,^{1,12} Chung-Hui Yang,⁴ Irene Miguel-Aliaga,^{5,6} J. Simon Wiegert,² Michael J. Pankratz,¹ Alisson M. Gontijo,^{3,7} Albert Cardona,^{8,9,10} and Peter Soba^{1,2,13,*}

¹LIMES Institute, Department of Molecular Brain Physiology and Behavior, University of Bonn, Carl-Troll-Str. 31, 53115 Bonn, Germany

²Center for Molecular Neurobiology (ZMNH), University Medical Center Hamburg-Eppendorf, Falkenried 94, 20251 Hamburg, Germany

³Integrative Biomedicine Laboratory, CEDOC, Chronic Diseases Research Center, NOVA Medical School, Faculdade de Ciências Médicas, Universidade Nova de Lisboa, Rua do Instituto Bacteriológico 5, 1150-082 Lisbon, Portugal

⁴Department of Neurobiology, Duke University Medical School, 427E Bryan Research, Durham, NC 27710, USA

⁵MRC London Institute of Medical Sciences, Du Cane Road, London W12 0NN, UK

⁶Institute of Clinical Sciences, Faculty of Medicine, Imperial College London, Du Cane Road, London W12 0NN, UK

⁷The Discoveries Centre for Regenerative and Precision Medicine, Lisbon Campus, Av. Rovisco Pais, 1049-001 Lisbon, Portugal

⁸HHMI Janelia Research Campus, 19700 Helix Drive, Ashburn, VA 20147, USA

⁹MRC Laboratory of Molecular Biology, Francis Crick Avenue, Cambridge CB2 0QH, UK

¹⁰Department of Physiology, Development, and Neuroscience, University of Cambridge, Downing Street, Cambridge CB2 3EJ, UK

¹¹Present address: Key Laboratory of Brain, Cognition, and Education Sciences, Ministry of Education, and Institute for Brain Research and Rehabilitation, South China Normal University, 510631 Guangzhou, China

¹²Present address: Department of Zoology, University of Cambridge, Downing Street, Cambridge CB2 3EJ, UK

¹³Lead contact

*Correspondence: psoba@uni-bonn.de

<https://doi.org/10.1016/j.cub.2021.10.069>

SUMMARY

Animals display selective escape behaviors when faced with environmental threats. Selection of the appropriate response by the underlying neuronal network is key to maximizing chances of survival, yet the underlying network mechanisms are so far not fully understood. Using synapse-level reconstruction of the *Drosophila* larval network paired with physiological and behavioral readouts, we uncovered a circuit that gates selective escape behavior for noxious light through acute and input-specific neuropeptide action. Sensory neurons required for avoidance of noxious light and escape in response to harsh touch, each converge on discrete domains of neuromodulatory hub neurons. We show that acute release of hub neuron-derived insulin-like peptide 7 (Ilp7) and cognate relaxin family receptor (Lgr4) signaling in downstream neurons are required for noxious light avoidance, but not harsh touch responses. Our work highlights a role for compartmentalized circuit organization and neuropeptide release from regulatory hubs, acting as central circuit elements gating escape responses.

INTRODUCTION

Animals use stimulus-specific, optimized strategies to deal with acute threats and noxious stimuli, including escape or avoidance behaviors.^{1–3} In the somatosensory system of vertebrates and invertebrates, noxious stimuli are sensed by nociceptive neurons, and their activation results in acute escape or avoidance.^{4–7} A specific noxious stimulus thereby elicits a stereotyped response with high fidelity (e.g., jumping in mice, corkscrew-like rolling in *Drosophila* larvae in response to noxious heat).^{6,8} Selection of the appropriate behavioral response minimizes risk and increases the likelihood of survival.

The neuronal networks underlying escape responses range from simple reflex to extensive circuits.^{8–13} Recent reconstruction of such networks at the synaptic level and neuronal circuit mapping have revealed extensive integration and interaction of circuits mediating distinct responses.^{8–10,14} Integration and

processing of sensory information starts at the sensory level, where different types of sensory neurons are converging on common second-order neurons, which are in turn part of the interconnected circuits providing feedback and feedforward information. How such circuits can specifically gate stimulus-specific information to support selected actions is not fully understood and difficult to deduce from pure anatomical network connectivity. Selection of behavior can occur probabilistically in a “winner takes all” fashion, for example, by reciprocal inhibition of circuits regulating mutually exclusive behaviors.^{10,15} Differences in the activation pattern of sensory neuron subsets can result in different sensations and behavioral responses, as shown for combinatorial coding in mechanosensation and olfaction, suggesting extensive integration and processing in such networks.^{16–19} Adding to the complexity of circuit computation are neuropeptides, which are expressed by many neurons across species.^{20–23} They can be released in parallel to small synaptic

neurotransmitters to exert modulatory functions.^{24–27} In most cases, their precise role, site of release, and action remain unclear, although they strongly contribute to network function and behavior.

To achieve detailed insight into the encoding of discrete escape responses at the circuit and neuromodulatory levels, we took advantage of the escape behavior of *Drosophila* larva, given its experimental accessibility and the ability to map the neuronal wiring diagram with nanometer resolution. The recent reconstruction of *Drosophila* larval brain circuits^{14,28,29} has revealed a complex somatosensory network capable of processing different mechanical and noxious stimuli^{14,30–32} comparable to its vertebrate counterpart.^{33–35} At the sensory level, class IV dendritic arborization (C4da) neurons are polymodal neurons able to detect noxious touch, heat, and UV/blue light, which generate two different escape behaviors^{6,36,37}: heat and harsh mechanical touch (mechanonociception) cause corkscrew-like rolling, while exposure to UV or blue light results in reorientation, avoidance, and dark preference. *Drosophila* larvae can sense UV, blue, and green light via different light-sensitive cells: Bolwig's organ (BO) consists of a group of cells in the larval head region and is sensitive to all of these wavelengths;³⁸ C4da neurons detect only noxious short-wavelength light in the UV and blue spectral range, presumably via the light-sensitive Gr28b receptor.³⁷ Avoidance responses to noxious light in acute and two-choice light-avoidance assays have been shown to rely on both BO and C4da neuron function.^{36,37} While the circuit mechanism for light avoidance has not been studied in detail thus far, mechanonociception requires the integration of three mechanosensory subtypes (namely C2da, C3da, and C4da) by dorsal pair insulin-like peptide 7 (Dp7) neurons,³⁹ which provide neuropeptidergic feedback via short neuropeptide F (sNPF). sNPF action in turn promotes C4da and downstream partner (A08n) neuron responses, thus facilitating rolling escape behavior.³⁰ As Dp7 neurons integrate input from the mechanosensitive and light-sensitive C4da neurons and have neuromodulatory functions, we reasoned that they are potential candidates for computing distinct behavioral outputs, depending on the type of sensory input.

RESULTS

Neuromodulatory Dp7 neurons integrate sensory input required for noxious light avoidance

To explore the larval somatosensory escape circuit for noxious light avoidance (Figures 1A and 1B), we sought to confirm the noxious effect of short-wavelength light on development by rearing freshly hatched larvae either under blue or green light (470 or 525 nm at 2.5 $\mu\text{W}/\text{mm}^2$). Only blue light exposure resulted in lethality during development at larval or white pupal stages (Figure 1C). Thus, *Drosophila* larvae may have evolved avoidance behaviors to avoid short-wavelength light (e.g., bright sunlight) during their development. We therefore explored the circuits underlying escape behavior in response to noxious light using a two-choice preference assay^{36,40} in which larvae in an arena were allowed to choose between darkness or white light of physiological relevance (365–600 nm with 6.9–3.3 $\mu\text{W}/\text{mm}^2$, respectively). After placing larvae close to the dark/light boundary, controls (w^{1118}) preferentially redistributed to the dark side

within <5 min and maintained this preference for at least 15 min (Figures S1A and S1B; Video S1). This allowed us to reliably assess light avoidance by analyzing larval distribution after 15 min as previously described³⁶ (see STAR Methods for details).

To test for a potential function of Dp7 neurons in noxious light avoidance, we genetically hyperpolarized them by expressing the inward rectifying potassium channel Kir2.1 (*Dp7-LexA*³⁰). In contrast to controls, silencing of Dp7 neurons strongly impaired larval light avoidance (Figures 1D, S1C, and S1D). We next tested whether Dp7 neurons were functionally activated in response to noxious light by expressing the calcium sensor GCaMP7s.⁴¹ To prevent crosstalk of the stimulus with excitation/emission of the sensor, we used a narrow 365-nm light pulse (10 s, 60 $\mu\text{W}/\text{mm}^2$). We found that UV light exposure gave rise to robust calcium responses in the soma of Dp7 neurons in live larvae (Figure 1E; Video S2), strongly suggesting that Dp7 neurons are part of an innate noxious light-sensing circuit.

We next asked whether Dp7 neuron-derived neuropeptides are involved in noxious light avoidance. Dp7 neurons express multiple neuropeptides, including sNPF and insulin-like peptide 7 (Ilp7), of which sNPF, but not Ilp7, is required for mechanonociception.^{30,42} Interestingly, we found that light avoidance was impaired in *Ilp7*^{ko}, but not sNPF mutant animals (Figure 1F). Temporal analysis showed that larvae eventually distributed almost evenly across the arena, suggesting that they are not able to maintain dark preference (Figures S1A and S1B). We analyzed light-dependent changes in larval locomotion in the dark or during exposure to noxious blue light. Control larvae displayed mildly elevated locomotion speed in blue light conditions, with a concomitant reduction in turning rates, presumably to escape the uniform noxious stimulus (Figures S1E and S1F). In contrast, *Ilp7*^{ko} animals displayed comparable speed, but lower turning rates in darkness, while slowing down and increasing turning under noxious light conditions. This suggests that in the absence of Ilp7, noxious light is still inducing locomotion changes, but responses are virtually inverted compared to controls. *Drosophila* larvae maintain light avoidance throughout development and preferentially pupariate in the dark.³⁶ *Ilp7*^{ko} animals formed pupae slightly earlier than controls (median *Ilp7*^{ko}: 119 h AEL, w^{1118} : 121 h AEL), but displayed reduced preference for pupariation in the dark (Figures S1G and S1H), suggesting that Ilp7 is required for light avoidance throughout development. Lastly, we rescued Ilp7 expression in *Ilp7*^{ko} animals using a Dp7 neuron-specific line, which completely restored light avoidance (*Dp7-Gal4* > *UAS-Ilp7*; Figures 1G and S1I). These data show that Dp7 neuron function and Ilp7 are required and that Dp7 neuron-derived Ilp7 is sufficient for noxious light avoidance.

Dp7 neurons integrate noxious light input from multiple somatosensory subcircuits

To gain more insight into the larval noxious light circuit, we identified the partially reconstructed Dp7 neurons from the electron microscopy (EM) brain volume of the first-instar larva.^{14,24} To confirm dendritic and axonal compartments of Dp7 neurons, we expressed a dendritic marker (DenMark⁴³) that labeled its medial and lateral arbors within the ventral nerve cord (VNC), but not the ascending arbor projecting to the brain lobes (Figure S2A). We then reconstructed Dp7 neurons and traced all of their synaptic partners (Figures 1H and S2B–S2F). Dp7 neurons

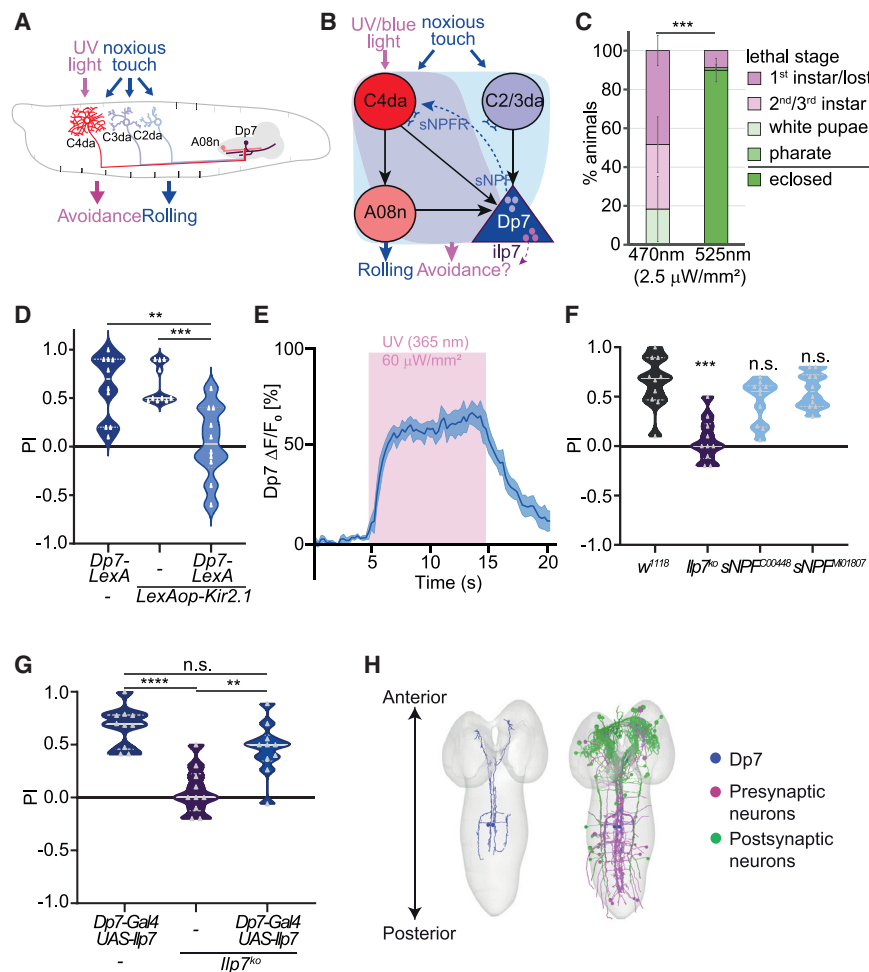


Figure 1. Ilp7-releasing Dp7 neurons are required for light avoidance

(A) Schematic representation of escape behaviors in *Drosophila* larvae. Noxious touch requires C2da, C3da, and C4da neurons for rolling escape, while noxious light sensed by C4da neurons elicits avoidance behavior.

(B) For mechanonociception, Dp7 neuron-derived sNPFF, but not Ilp7, enables mechanonociceptive rolling through feedback action on C4da neurons to facilitate output to A08n.³⁰

(C) Developmental lethality due to exposure to blue light (470 nm), but not green light (525 nm), of the same intensity (2.5 $\mu\text{W}/\text{mm}^2$). Percentage of freshly hatched larvae placed on food plates at 25°C dying at stages, as indicated in the legend (n = 5 trials, 50 larvae each, \pm SD; ***p < 0.0001, χ^2 test).

(D) Inactivation of Dp7 neurons using *LexAop-Kir2.1* under the control of *Dp7-LexA*, impairs larval light avoidance (n = 10 trials, **p < 0.01, ***p < 0.001, one-way ANOVA with Tukey's post hoc test).

(E) UVA light induces calcium transients in Dp7 neurons (*Ilp7-Gal4>UAS-GCaMP7s*, 365 nm, 60 $\mu\text{W}/\text{mm}^2$, means \pm SEMs indicated by shaded area, n = 4).

(F) *Ilp7^{ko}*, but not *sNPF* mutant animals, showed decreased light avoidance (n = 10 trials, ***p < 0.001; n.s., non-significant; one-way ANOVA with Tukey's post hoc test).

(G) Dp7 neuron-specific UAS-Ilp7 expression (with *Dp7-Gal4*) in the *Ilp7^{ko}* background restores light avoidance (n = 10 trials, *p < 0.05, ****p < 0.0001, one-way ANOVA with Tukey's post hoc test, *Ilp7^{ko}* dataset same as in E).

(H) EM-reconstructed Dp7 neurons and their highest connected synaptic partners. Upstream partners are shown in magenta, downstream partners in green.

See also [Figures S1](#) and [S2](#) and [Videos S1](#) and [S2](#).

receive most of the synaptic input in the VNC and provide output mostly in the subesophageal zone (SEZ) and brain lobe region along its dorsally projecting axon ([Figures 1H](#) and [S2C–S2F](#)). Dp7 neurons receive input from several subtypes of sensory neurons in the VNC ([Figures 1H](#) and [S2E](#)), suggesting that they are a somatosensory hub. We confirmed connectivity of Dp7 neurons with somatosensory neurons (C2da, C3da, C4da) as well as with C4 da neuron-connected A08n neurons³⁰ at the EM level ([Figure S2E](#)). Moreover, we identified a subset of tracheal dendrite (called *v'td2*⁴⁴) neurons as the sensory class with the highest Dp7 neuron connectivity ([Figures S2D](#) and [S2E](#)). In contrast, the anatomically similar subset of *v'td1* neurons was only weakly connected to Dp7 neurons at the connectome level ([Figures S2D](#) and [S2E](#); see also [Figure 2A](#)). Overall, four sensory circuits were found to converge on Dp7 neurons ([Figures 2A](#) and [2B](#)): direct monosynaptic connections from C4da and *v'td2* to Dp7 neurons and two 2-hop polysynaptic pathways. We identified a strong link via A08n neurons previously shown to receive numerous synaptic inputs from C4da neurons.^{28,30,45} Furthermore, the *v'td2* to Dp7 neuron link was strongly interconnected via so-far uncharacterized midline projection (MIP) neurons ([Figures 2A](#) and [S3A–S3D](#)).

As C4da neurons respond to UV and blue light and are involved in light avoidance,^{36,37} we tested whether A08n neurons as a major downstream output connected to Dp7 neurons may play a role as well. Unlike silencing of C4da neurons or ablation of BO, A08n neuron silencing did not result in significantly decreased light avoidance ([Figures S3E](#) and [S3F](#)). However, we detected robust calcium transients in A08n neurons in response to UV light ([Figure S3G](#)). Therefore, A08n neurons may only play a minor role in larval light avoidance, suggesting that C4da neurons may contribute to noxious light avoidance via other pathways.

v'td2 neurons are the major presynaptic partner of Dp7 neurons and co-labeled with C4da neurons by a reporter line of the putative light sensor Gr28b,^{37,44} suggesting a role in noxious light sensing. We confirmed synaptic and functional connectivity between *v'td2* and Dp7 neurons using a *v'td2*-specific Gal4 line (*73B01-Gal4*,⁴⁴ called *v'td2-Gal4* hereafter). Synapse-specific GFP reconstitution across synaptic partners (SybGRASP⁴⁶) showed that *v'td2*s form synaptic contacts with Dp7 neuron lateral dendritic arbors and along the proximal axonal segment ([Figure S3H](#)). Consistently, we also detected robust Dp7 neuron calcium responses upon optogenetic activation of *v'td2* neurons

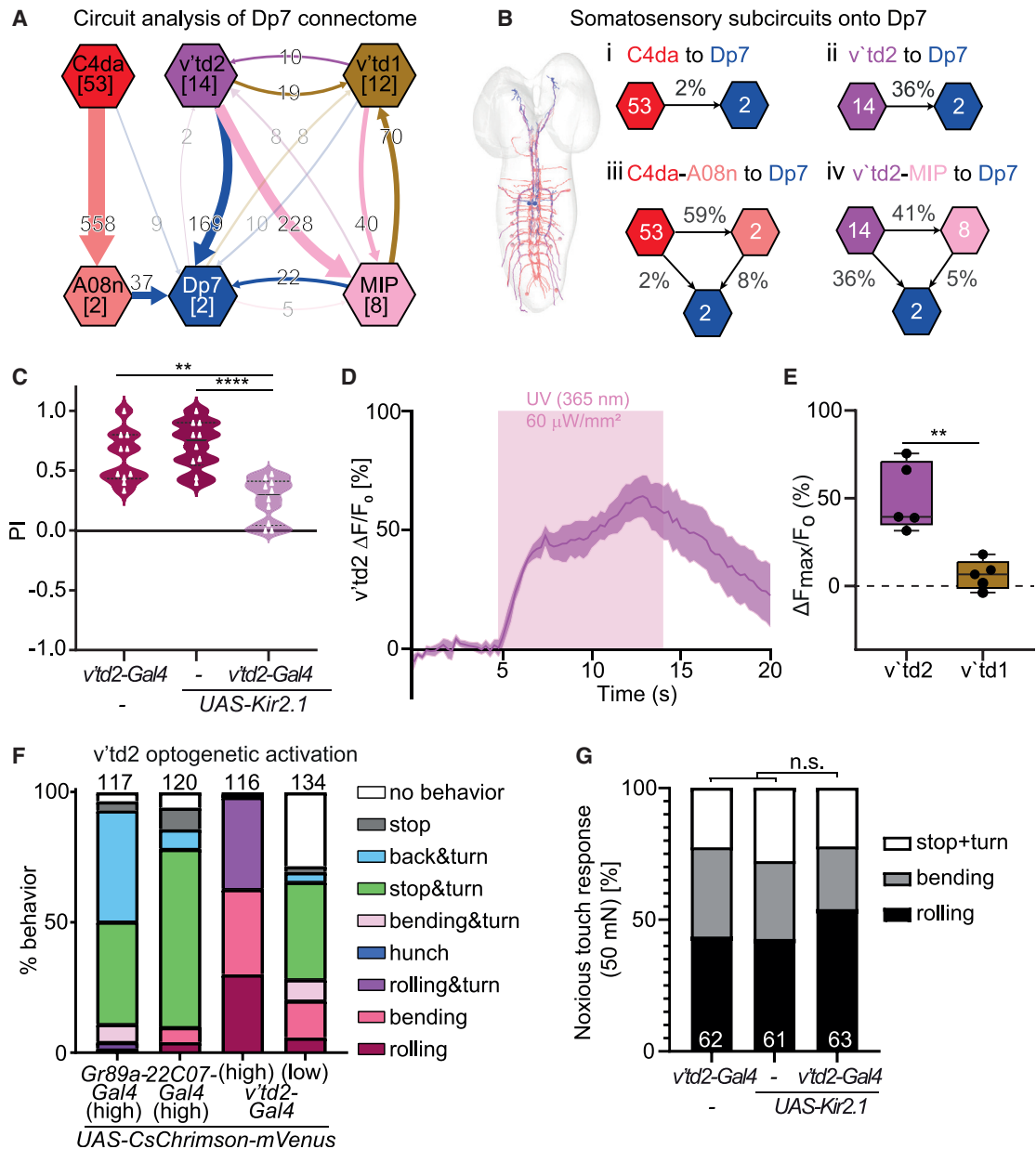


Figure 2. Dp7 integrates noxious light input from multiple somatosensory circuits

(A) Dp7 neuron presynaptic connectivity analysis showing the highest input from sensory v'td2 neurons. C4da to Dp7 neuron direct connectivity is weak, but additional indirect connections were found via A08n neurons. v'td2 neurons are additionally strongly connected to Dp7 neurons via MIP neurons, while v'td1 neurons display weak connectivity with Dp7 neurons and other circuit elements. Numbers in brackets indicate the number of neurons of the respective subtype; the numbers on the arrows indicate synapses from each neuronal subset forming direct connections.

(B) Inputs onto Dp7 neurons originating from either C4da or v'td2 neurons create 2 direct and 2 indirect subcircuits. The percentages of overall synaptic input of the target cells are shown.

(C) Silencing of v'td2 neurons using *Kir2.1* impairs light avoidance ($v'td2-Gal4 > UAS-Kir2.1$, $n = 10$ trials, $**p < 0.01$, $****p < 0.0001$, one-way ANOVA with Tukey's post hoc test).

(D) UV light-induced calcium transients in v'td2 neurons ($v'td2-Gal4 > GCaMP6s$, means \pm SEMs, $n = 8$).

(E) Quantitative comparison of calcium responses (GCaMP6s) of v'td2 and v'td1 neurons to UV light using *R35B01-Gal4*, which labels both subtypes ($\Delta F_{max}/F_0$ boxplot, $n = 5$, $**p < 0.01$, unpaired two-tailed t test).

(F) Optogenetic activation of CsChrimson (635 nm, high: $8.13 \mu W/mm^2$, low: $1.33 \mu W/mm^2$) using different previously characterized Gal4 driver lines expressing in v'td2 neurons.⁴⁴ Behavioral responses included avoidance (stop, backward, turn, hunch) and nocifensive behaviors (bending and rolling), as well as different combinations (n as indicated for each genotype). Note that all of the lines showed high prevalence for stop and turn or backward behavior depending on the activation level.

(G) Mechanonociceptive behavior (rolling and bending) is not affected by silencing of v'td2 neurons ($v'td2-Gal4 > UAS-Kir2.1$, $n =$ number of animals as indicated in graph, χ^2 test).

See also [Figures S2](#) and [S3](#) and [Videos S3](#) and [S4](#).

with CsChrimson (Figure S3I). We then tested whether v'td2 neurons are required for larval light avoidance. Similar to Dp7 neurons, Kir2.1-mediated silencing of v'td2 neurons significantly impaired light avoidance (Figure 2C). We further carried out calcium imaging of v'td2 neurons in intact larvae, which showed, similar to C4da neurons, acute responses to UV light stimulation (Figure 2D; Video S3). v'td1 sensory neurons, however, did not show calcium responses to UV stimulation (Figure 2E; Video S3), which is in line with the low connectivity to the Dp7 network (Figure 2A). We then tested whether v'td2 neurons could mediate acute avoidance behavior in response to optogenetic activation. We expressed and activated CsChrimson using different lines labeling v'td2 neurons, which resulted mostly in stop and turn or backward locomotion responses (Figure 2F; Video S4). At high, but not low, activation intensities, one of the three v'td2 lines used also induced significant rolling responses, likely due to the strong expression of CsChrimson. While we cannot rule out that v'td2 neuron activation can result in nociceptive rolling, Kir2.1-mediated silencing with the same driver line did not affect mechanonociceptive behavior, including rolling escape responses (Figure 2G). Thus, in contrast to C4da or A08n neurons, which are required for nociceptive rolling responses toward noxious touch,³⁰ v'td2 neuron activation induces acute avoidance behavior and is required for noxious light avoidance but not mechanonociception. Together with our connectome analysis, these findings show that at least two sensory subcircuits, C4da-A08n and v'td2 neurons, converge on Dp7 neurons and are involved in somatosensory UV light sensing, with v'td2, but not A08n neurons, strongly contributing to noxious light-avoidance behavior.

Compartmental organization of Dp7 hub neurons

To identify members of the noxious light-avoidance circuit downstream of Dp7 neurons, we analyzed the reconstructed synaptic wiring diagram. We identified abdominal leucokinin (ABLK) neurons, which receive direct input from Dp7, plus strong 2-hop synaptic connections from v'td2 via MIP neurons (Figure 3A). We inspected the topographical relationship of the mapped neurons and found that v'td2, MIP, and ABLK neurons anatomically converge on the ventrolateral dendritic arbor of Dp7 neurons (Figure 3B), which extends along the ventrolateral neuropil (Figure S4A). MIP and v'td2 neurons further extend mediodorsally along the axonal arbor of Dp7 neurons in the thoracic segments of the larval VNC and SEZ (Figures S3C and S3D). However, 75%–100% of synapses of v'td2 to MIP or Dp7 and MIP to ABLK neurons reside on the Dp7 ventrolateral dendrite (Figures 3B and 3C). This suggests the convergence of noxious light inputs and outputs within this Dp7 domain. In contrast, the mechanonociceptive circuit comprising C2da, C3da, C4da, and A08n neurons,³⁰ of which C4da and A08n also process noxious light information, primarily provides synaptic inputs on the medioventral dendritic arbor of Dp7 neurons (Figures 3D and S4A). Within the lateral region, Dp7 neurons receive extensive synaptic input from v'td2 neurons, which form concurrent (polyadic) synapses with MIP neurons. MIP neurons, in turn, innervate adjoining ABLK neuron processes also extending along the ventrolateral neuropil (Figures 3E, S4B, and S4C). This suggests that v'td2-MIP-ABLK neurons form a functional unit with the Dp7 ventrolateral arbor

and that processing of mechanonociceptive and noxious light information may preferentially occur in distinct Dp7 arbor domains.

Interestingly, the synaptic contact region of v'td2-MIP-ABLK neurons on the lateral arbor of Dp7 neurons also coincides with *llp7* neuropeptide localization (Figures 3B and 4A), suggesting that this could be a site of local peptide release. Analysis of Dp7 neurons in the EM volume revealed in total five putative fusion events of large dense-core vesicles (LDCVs), one of them occurring from Dp7 neurons to neighboring ABLK neurons (Figure 3F, arrow, from region marked with asterisk in Figure 3B). This indicated the possibility that *llp7* is released from Dp7 neurons in direct vicinity of ABLK neurons.

Dp7- and *llp7*-dependent output to ABLK neurons in response to noxious light

Based on their converging input from the noxious light-sensing circuit, we next asked whether ABLK neurons are relevant downstream outputs. We silenced leucokinin (*Lk*)-expressing neurons (*Lk-Gal4*⁴⁷) by expressing Kir2.1 and performed light-avoidance assays, which resulted in a strongly decreased dark preference (Figure 4B). As *Lk* is expressed in additional neurons in the SEZ (SELK) and brain lobes (ALK and LHKL), we genetically suppressed the expression of Kir2.1 only in ABLK neurons (*tsh-Gal80*; Figure S4H). Silencing of the remaining *Lk*⁺ neurons did not result in light-avoidance defects, suggesting a specific dependence on ABLK neuron function. We also tested Hugin-VNC neuron function in light avoidance, which are downstream partners of Dp7 neurons, but receive major sensory input from non-UV responsive v'td1 neurons (Figure 3A). Consistent with our connectome and functional analysis, we did not detect any significant defects when silencing Hugin-VNC neurons with a specific *Gal4* line⁴⁸ (Figure 4B). Our results show that ABLK neurons, but not Hugin-VNC neurons, are specifically involved in noxious light avoidance.

We analyzed potential light-dependent locomotion changes when silencing v'td2, *llp7*, or ABLK neurons. The average locomotion speed in the dark or during noxious blue light illumination was comparable to that of the control (Figure S4D), but overall turning rates of the animals, particularly during noxious light exposure, were reduced (Figure S4E). This indicated impaired reorientation/turning behavior under noxious light conditions. However, loss of *llp7* or silencing of v'td2, *llp7*, or ABLK neurons did not impair chemotaxis toward ethyl butyrate (Figures S4F and S4G), suggesting that complex navigational behavior is not generally affected. We next attempted to dissect ABLK neuron-dependent acute behavior by optogenetic activation of different *Lk*⁺ subsets (Figures S4H and S4I). While we could selectively block expression in ABLK or brain lobe (ALK and LHKL) neurons using different genetic approaches, we could not suppress expression in SELK neurons. Optogenetic activation resulted in consistently strong rolling responses, suggesting that SELK neurons are likely involved in nociceptive rolling (Video S5).

We then assayed ABLK neuron responses to UV light using GCaMP6s and found prominent calcium transients upon stimulation (Figures 4C and S5A; Video S2). In contrast, SELK neurons did not respond to UV light, strongly suggesting that they are not involved in noxious light avoidance (Figure S5B; Video S2). We further assessed the activation of ABLK neurons by different light

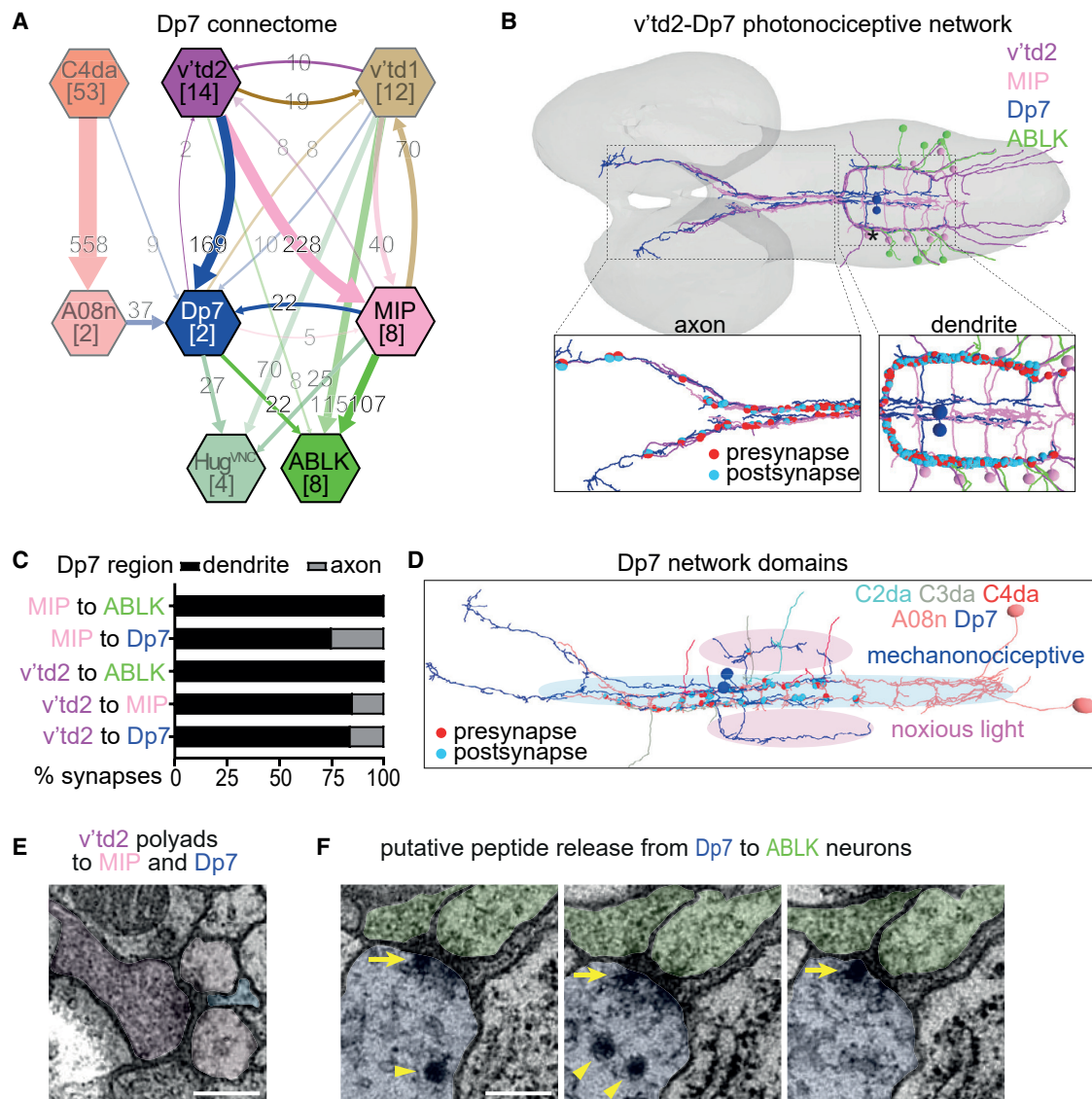


Figure 3. Domain-specific organization of the noxious light-avoidance network

(A) Connectivity graph of Dp7 neurons shows overlapping but distinct subcircuits. The major outputs of v'td2 neurons are Dp7 and MIP neurons, while v'td1 neurons strongly connect to ABLK and Hugin-VNC neurons. The numbers on the arrows indicate synapses from each neuronal subset forming direct connections.

(B) Overview of reconstructed Dp7, v'td2, MIP, and ABLK neuron innervation. Enlarged axon and dendrite regions of Dp7 neurons show local v'td2-Dp7, v'td2-MIP, and MIP-ABLK synapses on the lateral dendrite and anterior axon of Dp7 neurons.

(C) Relative synapse numbers in Dp7 dendritic and axonal arbor regions are shown for each partner.

(D) Synaptic connectivity of mechanosensory (C2da, C3da, C4da) and A08n neurons with Dp7. Most synapses are located on Dp7 medial dendrites providing mechanonociceptive input (indicated by shaded blue area). Except for C4da and A08n synapses, noxious light inputs (as shown in B) are mainly found on Dp7 lateral dendrites (indicated by shaded magenta area).

(E) v'td2 forms polyadic synapses with MIP and Dp7 neurons. Scale bar, 200 nm.

(F) Putative peptide release by docked LDCV (indicated by arrow) from Dp7 (blue) to adjacent ABLK neurons (green) in consecutive EM sections (region indicated by asterisk in B); additional LDCVs indicated by arrowheads. Scale bar, 200 nm.

See also Figure S4.

intensities and wavelengths using the red-shifted calcium sensor jRCaMP1b.⁴⁹ We could detect strong and acute calcium transients in ABLK neurons at UV light intensities ranging from 20 to 60 $\mu\text{W}/\text{mm}^2$ (Figure S5C). We then illuminated with different wavelengths in a range from 365 to 525 nm with the same

intensity (60 $\mu\text{W}/\text{mm}^2$), revealing strong responses up to 470 nm, but not at 525 nm (Figure S5D). These data show that ABLK neurons are responding only to light within the noxious UV and blue wavelength range and that they are a part of a noxious light-sensing circuit.

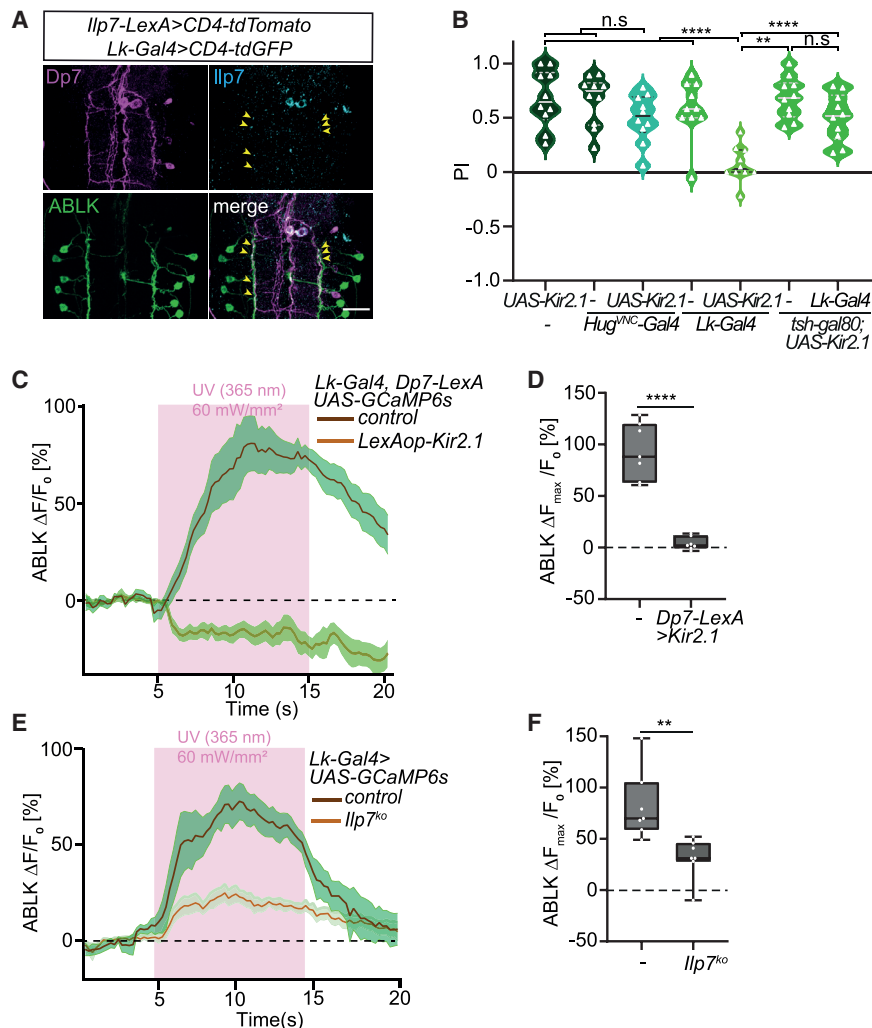


Figure 4. Dp7 neuron activity and *Ilp7* peptide are required for noxious light information flow to ABLK neurons

(A) Confocal image stack (maximum projection) showing anatomical overlap of ABLK (*Lk-Gal4 > UAS-CD4-tdGFP*) and *Ilp7* neuropeptide puncta (cyan) along the lateral dendritic region of Dp7 neurons (*Ilp7-LexA > LexAop-CD4spGFP11-tdTomato*). Scale bar, 50 μ m.

(B) Silencing of LK neurons (*Lk-Gal4 > UAS-Kir2.1*), but not when precluding ABLK expression (*tsh-Gal80, Lk-Gal4 > UAS-Kir2.1*), abolishes light avoidance. Silencing Hugin-VNC neurons (*Hug^{VNC}-Gal4 > UAS-Kir2.1*) does not affect light avoidance ($n = 10$ trials/genotype, **** $p < 0.0001$, ** $p < 0.01$, one-way ANOVA with Tukey's post hoc test).

(C) ABLK neuron calcium transients evoked by UV light with or without Dp7 neuron silencing (*Dp7-LexA, LexAop-Kir2.1*, means \pm SEMs, $n = 7$).

(D) Boxplot quantification (% $\Delta F_{max}/F_0$) showing ABLK neuron response to UV light (*Lk-Gal4 > UAS-GCaMP6s*) with or without *Ilp7* neuron silencing (*Ilp7-LexA > LexAopKir2.1*, $n = 7$ larvae/genotype, **** $p < 0.0001$, unpaired t test).

(E) ABLK neuron calcium transients evoked by UV light in control and *Ilp7^{ko}* animals (means \pm SEMs, $n = 7$).

(F) % $\Delta F_{max}/F_0$ boxplots ($n = 7$ larvae/genotype, unpaired t test, ** $p < 0.01$).

See also [Figures S4](#) and [S5](#) and [Videos S2](#) and [S5](#).

We next examined whether ABLK neuron responses to noxious light depend on Dp7 neuron function. To this end, we silenced Dp7 neurons using *Kir2.1* expression and monitored ABLK neuron responses to UV light, which were absent under these conditions ([Figures 4C](#) and [4D](#)). To assay whether Dp7-derived *Ilp7* was required for ABLK activation, we performed calcium imaging in *Ilp7^{ko}* animals and detected a 70% decrease in ABLK neuron responses after UV light stimulation ([Figures 4E](#) and [4F](#)). In contrast, the expression of tetanus toxin light chain (TNT) in Dp7 neurons did not affect ABLK neuron responses to UV light ([Figure S5E](#)), suggesting that synaptic transmission from Dp7 to ABLK neurons does not play a major role in this context. However, we cannot exclude the involvement of other neuropeptides contributing to ABLK responses. To test for a contribution to ABLK neuron activation by other light-sensing pathways, including C4da neurons or BO, we blocked their function by TNT expression or genetic ablation (*GMR-hid*), respectively. In both cases, ABLK neuron responses to UV light were not significantly impaired ([Figure S5E](#)). Similarly, the optogenetic activation of Dp7, BO, or C4da neurons using *CsChrimson* did not result in a significant activation of ABLK neurons, suggesting that neither Dp7 nor BO or C4da neurons are sufficient to activate ABLK

neuron activation by noxious light, which likely involves the v'td2-MIP-Dp7 circuit rather than C4da neurons or BO.

Acute *Ilp7* release from Dp7 neurons in response to noxious light

We next investigated the peptidergic link between Dp7 and ABLK neurons in more detail by asking whether *Ilp7* release from Dp7 neurons can be acutely induced by UV light stimulation. We generated an *Ilp7* release reporter by fusing *Ilp7* to *GCaMP6s* (*NPRR^{Ilp7}*), analogous to previously characterized neuropeptide reporters.⁵⁰ *NPRR^{Ilp7}* expressed in Dp7 neurons localized in a punctate pattern similar to the endogenous pattern of *Ilp7*, and colocalized completely with the LDCV-specific Synaptotagmin *Syt α* ⁵¹ ([Figures S6A](#) and [S6B](#)). We next imaged *NPRR^{Ilp7}* responses to UV light in Dp7 neurons in live larvae. *NPRR^{Ilp7}* puncta in the proximal axon and ventrolateral dendrite region of Dp7 neurons displayed low baseline fluorescence consistent with low LDCV calcium levels, which increased rapidly upon UV light illumination, indicating peptide release ([Figures 5A](#) and [5B](#); [Video S6](#)). Repeated UV-light stimulation resulted in consistent *NPRR^{Ilp7}* responses in LDCV puncta ([Figures 5C](#) and [5D](#)). These data are compatible with acute and rapid

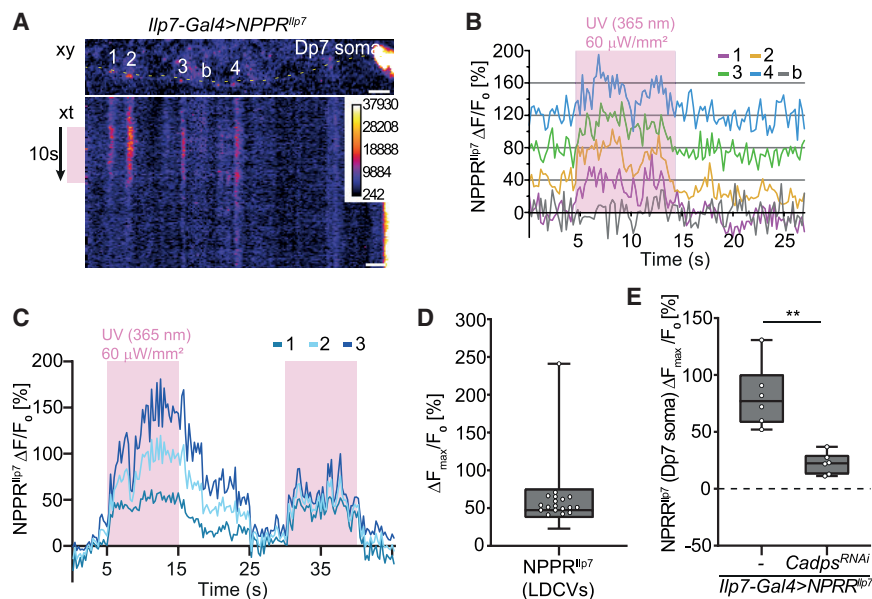


Figure 5. Acute Ilp7 peptide release from Dp7 neurons in response to UV light

(A) *NPPR^{Ilp7}*-labeled LDCVs (numbers 1–4; b, background) located along the Dp7 proximal axon. Time series (xt) along the dotted line showing acute evoked *NPPR^{Ilp7}* fluorescence increase in response to a 10-s UV light exposure (365 nm, 60 $\mu\text{W}/\text{mm}^2$). Scale bars, 10 μm . (B) Stacked individual traces of *NPPR^{Ilp7}*-labeled LDCVs (numbered 1–4, individual responses are stacked by 20% each for clarity) and background (b) shown in (A).

(C) Repeated UV light-induced responses of individual *NPPR^{Ilp7}* puncta located along the proximal axon or lateral dendrite of Dp7 neurons (from 3 representative experiments).

(D) $\Delta F_{\text{max}}/F_0$ boxplot of Dp7 *NPPR^{Ilp7}* responses to UV light ($n = 18$ LDCVs from 6 animals).

(E) Boxplot quantification (% $\Delta F_{\text{max}}/F_0$) of maximum *NPPR^{Ilp7}* fluorescence change in Dp7 somata upon UV light stimulation without or with *Cadps*-RNAi. *Cadps* knockdown significantly reduces *NPPR^{Ilp7}* responses ($n = 6$ larvae/genotype, $***p < 0.001$, unpaired t test). See also [Figure S6](#) and [Video S6](#).

peptide release by partial LDCV fusion with the plasma membrane in the millisecond-to-second range, similarly to kiss-and-run-type peptide release upon electrical stimulation.^{50,52} Imaging of *NPPR^{Ilp7}* in the Dp7 soma showed similar responses, also suggesting somatic release ([Figure S6C](#)). In contrast, posterior *Ilp7⁺* neurons, which innervate the gut, did not show UV light-induced somatic *NPPR^{Ilp7}* responses ([Figure S6C](#)). To further confirm that *NPPR^{Ilp7}* is reporting LDCV fusion with the plasma membrane, we used RNAi to knock down calcium-dependent secretion activator (*Cadps*), a conserved protein required for LDCV release, but not biogenesis.^{53,54} UV light-induced *NPPR^{Ilp7}* responses in the Dp7 soma were strongly diminished upon *Cadps*-RNAi, showing that the observed responses are LDCV release dependent ([Figure 5E](#)). Our data thus show that LDCVs containing *Ilp7* are acutely released from Dp7 in response to UV light, thereby acting directly on neighboring ABLK neurons, reminiscent of small-molecule neurotransmitter action.

Neuropeptidergic decoding of circuit responses and behavior for noxious light

As the noxious light and mechanonociceptive circuits overlap extensively at the sensory C4da and Dp7 neuron level, we asked whether *Ilp7*-dependent output of Dp7 to ABLK neurons is specific for UV light. Kir2.1-mediated silencing of LK neurons, with or without the inclusion of ABLK neurons, did not significantly impair mechanonociceptive escape responses resulting in nocifensive rolling behavior ([Figure 6A](#)). Instead, silencing all LK neurons mildly facilitated mechanonociceptive behavior, which is in line with a similar effect described for *Ilp7* deletion.³⁰ Moreover, in sharp contrast to UV light stimulation, we did not detect calcium responses in ABLK neurons after mechanonociceptive stimulation ([Figure 6B](#)). Divergence of the mechanonociceptive and noxious light circuits thus occurs downstream of Dp7 neurons through *Ilp7*-mediated actions on ABLK neurons.

While no cognate *Ilp7* receptor has been identified so far, the relaxin family receptor *Lgr4* has coevolved with *Ilp7* across

arthropod species, suggesting a receptor-ligand relationship.^{55,56} A *Gal4* reporter incorporated in the endogenous *Lgr4* mRNA (*Lgr4^{T2AGal4}*) displayed expression in ABLK neurons, suggesting the presence of *Lgr4* ([Figure 6C](#)). We further analyzed the localization of an ABLK-expressed hemagglutinin (HA)-tagged *Lgr4*, which localized along ABLK neuron projections close to endogenous *Ilp7* puncta present on the ventrolateral branch of Dp7 neurons ([Figure 6D](#)). In addition, we biochemically confirmed *Ilp7* and *Lgr4* interaction in S2 cells in co-immunoprecipitation assays showing that *Ilp7* and *Lgr4* are capable of binding *in vitro* ([Figure S6D](#)). Binding was dependent on the presence of the extracellular leucine-rich repeat (LRR) domain of *Lgr4*, but not a conserved residue (I263) required for interaction of the mammalian orthologs RXFP1 and relaxin ([Figure S6E](#)).

To find out whether *Lgr4* is physiologically relevant for noxious light avoidance, we tested *Lgr4^{T2AGal4}* larvae, which carry a T2A-*Gal4* exon, resulting in the loss of *Lgr4* as confirmed by qPCR analysis ([Figure S6F](#)). *Lgr4^{T2AGal4}* animals showed significantly reduced light avoidance, which could be fully rescued by the overexpression of *Lgr4* in its endogenous pattern ([Figure 6E](#)). We then imaged calcium responses of ABLK neurons using a confirmed *Lgr4* knockout (KO) allele (*Lgr4^{ko57}*) showing reduced light avoidance as well ([Figures 6F, 6G, S6G, and S6H](#)). Similar to *Ilp7^{ko}* animals, we detected a 3-fold decrease in calcium transients, which was rescued upon the expression of *Lgr4* only in *LK⁺* neurons, including ABLKs ([Figures 6F and 6G](#)). Collectively, these results suggest that *Lgr4* acts downstream of *Ilp7* in ABLK neurons to promote their UV light responses and light-avoidance behavior.

DISCUSSION

Noxious light processing in *Drosophila* larvae for sustained avoidance responses

All animals must detect noxious stimuli and engage in appropriate escape actions to avoid injury or death. Consistent with previous reports,^{58,59} extended exposure to blue, but not green,

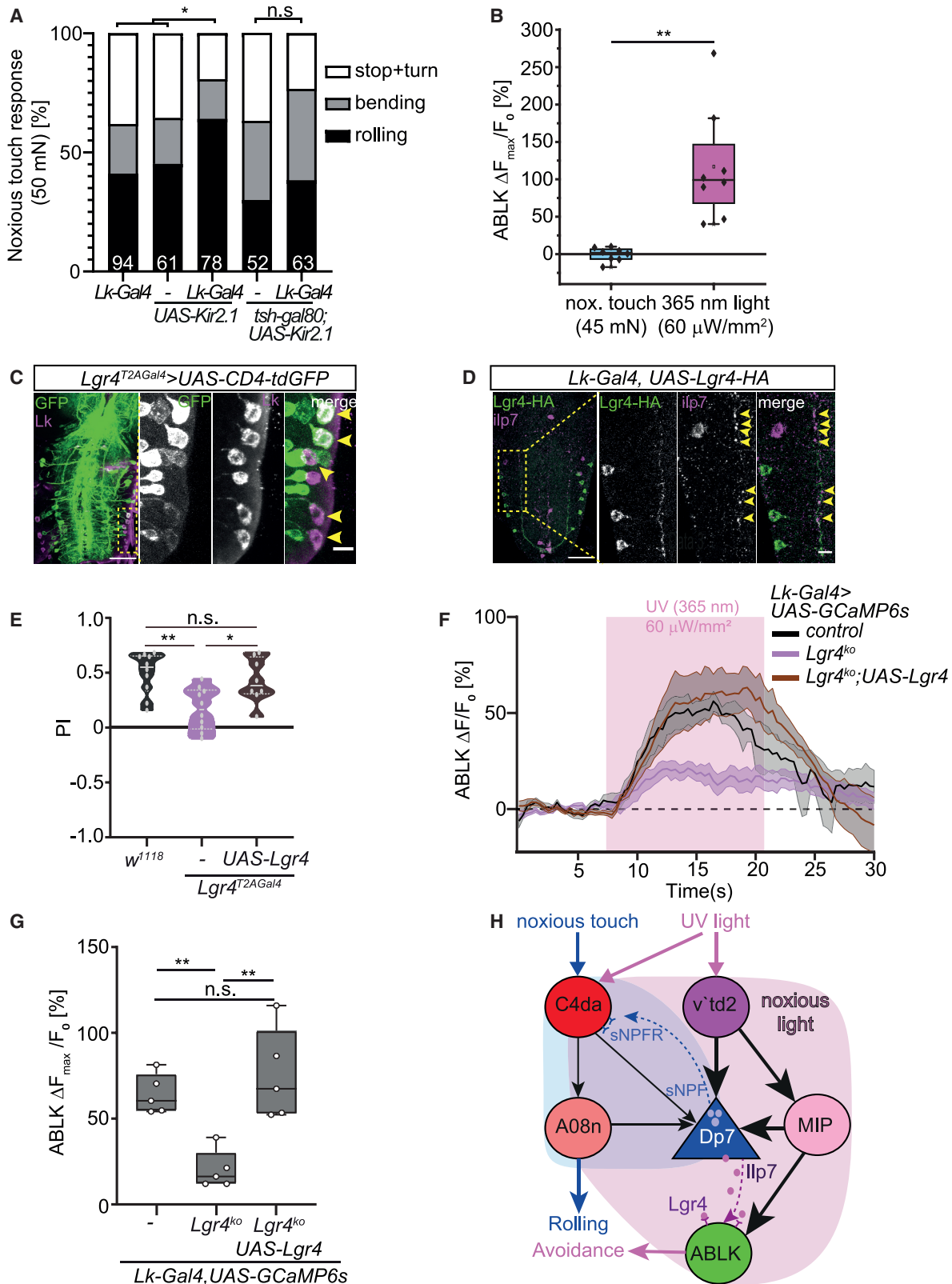


Figure 6. Neuromodulatory decoding of nociceptive escape behaviors

(A) Mechanonociceptive responses upon silencing of Lk neurons (*Lk-Gal4 UAS-Kir2.1*), with or without ABLK silencing (*Lk-Gal4;tsh-Gal80,UAS-Kir2.1*; n = total number of larvae indicated in graphs, * $p < 0.05$, χ^2 test).

(legend continued on next page)

light is noxious and lethal for developing *Drosophila* larvae. This suggests a strong need to efficiently detect and avoid short-wavelength light. Extraocular UV/blue light sensors expressed in body wall neurons have been identified in several invertebrates, including *Caenorhabditis elegans*⁶⁰ and *Drosophila*,^{37,61,62} and the underlying circuits seem to aid in the detection and avoidance of noxious light qualities and intensities. Previous work in *Drosophila* larva showed that besides BO, C4da neurons are involved in acute UV or blue light-avoidance responses,^{37,63,64} likely via independent circuits. Here, we provide evidence that v'td2 neurons represent an additional set of larval body wall neurons sensing noxious light and inducing avoidance responses via peptidergic Dp7 neuron action and ABLK neuron activation. Of note, ABLK neurons have been proposed to gate binary escape decisions in response to optogenetic activation of C4da neurons using a blue light-activated channelrhodopsin.⁶⁵ Our connectomic, functional, and behavioral data show that ABLK neurons are actually part of a UV and blue light-sensing circuit promoting acute and sustained noxious light-avoidance behavior. While ABLK neurons have known additional functions in stress response pathways^{66,67} and blue light-induced rearing behavior,⁶⁸ the lack of major connectivity and functional activation of ABLK by C4da neurons as shown in our work will require further investigation of their role in computing binary escape decisions.

Why do *Drosophila* larvae need three seemingly independent sensory circuits (BO, C4 da, and v'td2) to sense and avoid noxious light? BO is located in the larval head region, while v'td2 and C4 da neurons reside in abdominal segments (A1–A7) or tile the entire body wall,^{38,44,69} respectively. For acute noxious light responses after exposure on the larval head region, BO and C4da neurons seem to be jointly required.^{37,63} However, as shown for our v'td2-Dp7-ABLK circuit here and previously for BO⁴⁰ and C4da neurons,³⁶ each of these sensory units is necessary for efficient light avoidance in choice assays. Under such chronic conditions, the combined action of these sensory systems covering different larval body regions may enable a sustained behavioral mode for continuous avoidance of extended periods of noxious light exposure of any body part. Although we could not identify a connectomic or functional link between BO and the circuit described here, C4da neurons may still contribute to Dp7 neuron-dependent Ilp7 release based on their ability to promote Dp7 neuron activation in mechanonociception.³⁰ We cannot rule out additional outputs of v'td2 neurons besides ABLK neurons, which may reside within the MIP connectome. However, it is also possible that these

light-sensing circuits are connected via long-range peptidergic/hormonal regulation, as BO-dependent release of PTH (prothoracicotropic hormone) has been suggested to control C4da neuron function in light-avoidance behavior.³⁶ This indicates that global hormonal signals may additionally coordinate the action of these circuits.

Neuromodulatory hub-mediated sensory processing

The challenge of a nervous system is to generate the correct behavioral output, such as specific escape responses, based on the received sensory input. Emerging connectomic data from *Drosophila* illustrates that sensory networks fan out extensively, adding numerous partners at each subsequent level.^{14,28,70} As a result, the relevant output path of any given sensory input is often difficult to identify, indicating that physical connection is not a sufficient predictor for function.^{22,71} This suggests specific circuit mechanisms for selective gating of action-specific network components. Along these lines, a hub-and-spoke-like circuit has been identified in *C. elegans*, where the RMG neuron forms a hub that receives spoke-like input from several sensory neurons regulating aggregation behavior via neuromodulatory signaling.^{72,73} Similarly, somatostatin⁺ neurons in the spinal cord receive converging input from different mechanosensory pathways⁷⁴ and play a pivotal role in mechanical pain processing. Such convergence of multiple sensory inputs allows the integration and regulation of behavioral output, suggesting that neuropeptide-expressing neurons are local network hubs. In our work, Dp7 neurons act as a regulatory hub that gates the activation of specific network responses. This may be particularly important in sensory processing, in which peptidergic action can increase the computational power by organizing circuit function to generate alternative behaviors.^{22,27,75} In mice, alternative escape behaviors are regulated by competitive and mutually inhibitory circuits of corticotropin-releasing factor and somatostatin⁺ neurons in the central amygdala, which mediate conditioned flight or passive freezing, respectively.¹⁰ While direct involvement of these neuromodulators has not yet been shown, oxytocin release from presynaptic terminals of hypothalamic neurons in the central amygdala attenuates fear responses in mice,^{76,77} suggesting extensive neuromodulatory regulation of escape and related behaviors across species. Our work revealed that discrete escape pathways are controlled by Dp7 hub neurons through input-specific neuropeptide function. Rolling in response to noxious mechanical touch^{6,78} requires feedback signaling from Dp7 neurons via

(B) Maximum ABLK neuron responses (boxplot, % $\Delta F_{\max}/F_0$) to noxious mechanical or UV light stimulations in semi-intact live larval preparations ($n = 8$, unpaired t test, ** $p < 0.01$).

(C) Endogenous Lgr4 reporter expression (*Lgr4^{T2AGal4},UAS-CD4-tdGFP*) in ABLK neurons detected by colocalized anti-Lk immunostaining. Overview and magnified lateral VNC region (boxed region) with ABLK neuron somata (GFP: green, Lk: magenta). Scale bars, 50 μm , 10 μm for enlarged view.

(D) Lgr4-HA localization in ABLK neurons (*Lk-Gal4,UAS-Lgr4-HA*) with anti-Ilp7 immunostaining. Overview and magnified lateral VNC region (boxed region) showing ABLK neuron somata and dendrites with proximity of Lgr4 (green) and Ilp7 (magenta) puncta on the Dp7 neuron lateral arbor. Scale bars, 50 and 10 μm .

(E) *Lgr4^{T2AGal4}* animals display reduced light avoidance, which was rescued by *UAS-Lgr4* expression ($n = 10, 10$, and 8 trials/genotype; * $p < 0.05$, ** $p < 0.01$, one-way ANOVA with Tukey's post hoc test).

(F) GCaMP6s-expressing ABLK neuron responses to UV light in control and *Lgr4^{ko}* animals, with and without *UAS-Lgr4* expression (*Lk-Gal4 > GCaMP6s*, $n = 5$ animals/genotype, means \pm SEMs).

(G) Quantitative $\Delta F_{\max}/F_0$ boxplots of (F) ($n = 5$, ** $p < 0.01$, one-way ANOVA, with Tukey's post hoc test).

(H) Model depicting neural and molecular elements shaping the larval somatosensory escape circuit, with specific action of sNPF or Ilp7 on mechanonociception versus noxious light resulting in rolling or avoidance, respectively.

See also Figure S6.

sNPF, but not Ilp7 peptide.³⁰ In contrast, noxious light-avoidance behavior requires Dp7 neuron-derived Ilp7, but not sNPF, and acts via a feedforward mechanism. Circuit-specific neuropeptide action thus generates discrete escape behaviors in this system by creating divergent networks, despite the extensive overlap between mechanonociceptive and noxious light avoidance circuits (Figure 6H). This may raise the question of why these circuits are converging on hub neurons in the first place. First, sensory integration can facilitate escape responses as vibration¹⁴ or blue light⁷⁹ enhance nociceptive rolling in *Drosophila* larvae. Second, escape responses may have to be tuned depending on the overall environmental context as well as the state of the animal, for which peptidergic regulation is known to be a key factor.²²

Compartmentalized modality-specific circuits and neuromodulatory action

Specific compartmentalization of sensory inputs and outputs can increase the efficiency of network computation at hub neurons through combined local synaptic and neuropeptide domains. In *C. elegans*, peptide release from the PVD neuron dendrites provides local proprioceptive feedback to motor neurons.⁸⁰ Discrete functional domains have also been described for *Drosophila* mushroom body Kenyon cells displaying compartmentalized activity, which encodes context-specific functions by local dopaminergic modulation.^{81–83} Here, we show the convergence of UV light-responsive inputs and outputs with Ilp7 release sites on the Dp7 lateral dendritic arbor, which likely form a computational unit of the noxious light-avoidance circuit. Analogous compartmental organization is likely found in the somatosensory system of adult flies⁸⁴ and also in vertebrates displaying modality-specific laminar organization of sensory inputs and corresponding outputs.^{16,17,85} This suggests that integrating neuropeptide-expressing neurons receiving sensory input linked to distinct modalities, such as Dp7 neurons in *Drosophila* or somatostatin-expressing neurons in the vertebrate spinal cord,⁷⁴ play a pivotal role in processing sensory stimuli. Dendrites can act as independent computational units,⁸⁶ as shown in the vertebrate retina.⁸⁷ Although we could identify physical compartmentalization of input and output domains, most of the physiological responses, including peptide release, seem to occur globally across the entire neuron. We currently lack the tools and resolution to investigate region-specific differences in calcium levels or peptide release efficiency. Nonetheless, neuromodulatory signals can still aid local processing due to circuit-specific expression of cognate receptors, as shown here by noxious light-specific responses of Lgr4-expressing ABLK neurons. In line with this notion, neuropeptide overexpression studies in zebrafish have shown that sensory responsiveness can be regulated in a peptide- and modality-specific manner⁸⁸ suggesting that their signaling still acts on selective circuits to enhance respective innate behaviors. Thus, compartmentalized circuits with broad yet functional unit-specific neuromodulatory action may be a widespread mechanism to generate context-specific behaviors.

Neuropeptide-mediated co-transmission selects network action and behavior

Co-transmission of small-molecule neurotransmitters and neuropeptides has been described in vertebrates and

invertebrates;^{20,22,27,89} however, the acute signaling function of neuropeptides in sensory behavior is not well understood. In general, neuropeptide release has been described to occur upon neuronal activity,^{25,50,90–92} although their action is considered slow and broad,^{20,22} with the ability to regulate targets distant from release sites (e.g., opioid receptor signaling in stress-induced analgesia)⁹³ and long-lasting behavioral states, including sleep, foraging, and social behavior.^{72,94,95}

Here, we show that Ilp7 is acutely released from Dp7 neurons in response to noxious light and required for full ABLK neuron activation. Residual ABLK neuron calcium transients in the absence of Ilp7, likely due to small neurotransmitter activity in this network, are not sufficient for noxious light-avoidance behavior. This suggests that Ilp7 can act as a co-transmitter required for selective network activation and behavior. Ilp7 presumably acts via Lgr4 to enable noxious light-avoidance responses and behavior. Lgr4 belongs to the conserved family of relaxin receptors.^{55,96–100} Recent work indicates a role for relaxin-3 in escape behavior through the inhibition of oxytocin-producing neurons in the hypothalamus, a brain region implicated in the modulation of escape responses of vertebrates.^{76,101} This suggests a conserved role of relaxin signaling in escape responses.

Overall, our data suggest that neuropeptidergic signals can act acutely on the physical neuronal network to promote selective network activity and specific innate behaviors. Based on the widespread expression of neuropeptides and cognate G protein-coupled receptors (GPCRs), including in escape circuits,^{20–23,102} further studies must determine whether local neuromodulatory hubs with compartmentalized circuits as described here may be a general motif for the computation of modality-specific sensory responses.

STAR★METHODS

Detailed methods are provided in the online version of this paper and include the following:

- KEY RESOURCES TABLE
- RESOURCE AVAILABILITY
 - Lead contact
 - Materials availability
 - Data and code availability
- EXPERIMENTAL MODEL AND SUBJECT DETAILS
 - Fly stocks
 - S2-DRSC cell line
- METHOD DETAILS
 - Generation of plasmids and transgenes
 - Neuronal reconstruction and circuit mapping
 - Immunohistochemistry and confocal imaging
 - Developmental toxicity assay
 - Light avoidance assays
 - Mechanonociception assays
 - Locomotion and chemotaxis assays
 - Optogenetic behavioral assays
 - Calcium imaging in intact larvae
 - Calcium imaging in semi-intact larvae
 - Cell culture and co-immunoprecipitation assay
 - qRT-PCR

- Light avoidance pupariation assay
- Developmental time assay
- **QUANTIFICATION AND STATISTICAL ANALYSIS**
- Statistics
- Analysis of network synaptic counts
- Developmental toxicity assay
- Light avoidance analysis
- Mechanonociception analyses
- Locomotion and chemotaxis analysis
- Analysis of calcium imaging

SUPPLEMENTAL INFORMATION

Supplemental information can be found online at <https://doi.org/10.1016/j.cub.2021.10.069>.

ACKNOWLEDGMENTS

We would like to thank M. Petersen and A.R.M. Dias for excellent technical assistance; C. Wegener, T. Oertner, F. Morellini, J. Parrish, and Q. Yuan for comments on the manuscript; B. Ye, B. Hofbauer, and C. Wegener for communicating results prepublication; P. Herrero, C. Wegener, M. Wernet, and D. Anderson for fly stocks; T. Kazimierz for advice and troubleshooting with CATMAID; and L. Herren for supervising Dp7 connectome reconstruction. P. Soba, B.N.I., and A.C. thank the visiting scientist program at HHMI Janelia, and HHMI Janelia for funding. Stocks obtained from the Bloomington *Drosophila* Stock Center (NIH grant P40OD018537) and Vienna *Drosophila* Resource Center (VDRC; <http://stockcenter.vdrc.at>) were used in this study. cDNA and cells obtained from the *Drosophila* Genomics Resource Center (NIH grant 2P40OD010949) were used in this study. This work was supported by the Deutsche Forschungsgemeinschaft (DFG; SO1337/4-1, SO1337/2-1/2-2, and SO1337/7-1 to P. Soba; WI4485/2-2 and WI4485/3-2 to J.S.W.), the DFG Heisenberg program (SO1337/6-1 to P. Soba), an Alexander von Humboldt Research Fellowship (to A.F.), an EMBO Short-Term Fellowship (to E.M.V.), the European Commission FP7 (PCIG13-GA-2013-618847 to A.M.G.), the European Research Council Horizon 2020 (ERC2016-StG-714762 to J.S.W.), the FCT (IF/00022/2012; Congento LISBOA-01-0145-FEDER-022170, co-financed by FCT/Lisboa2020; UID/Multi/04462/2019, PTDC/BEXBCM/1370/2014, and PTDC/BIA-BID/31071/2017 to A.M.G.; PTDC/MED-NEU/30753/2017 to F.H. and A.M.G.; and SFRH/BPD/94112/2013 to A.M.), PD/BD/52421/2013 to F.H., and SFRH/BD/135263/2017 via PGCD (Programa Pós-Graduação Ciência Para o Desenvolvimento) to E.M.V.

AUTHOR CONTRIBUTIONS

B.N.I. performed and analyzed most of the experiments, including connectome reconstruction and analysis, phototoxicity assays, light-avoidance behavior analysis, calcium imaging, and morphological analysis, and wrote the manuscript. A.W. and F.Z. performed a subset of the light-avoidance assays. F.Z. and A.F. performed the locomotion and chemotaxis assays and analysis. A.F. wrote the custom analysis scripts and code. C.H. performed and analyzed experiments in semi-intact larval preparations. F.M.T. performed and analyzed the mechanonociceptive and optogenetic behavior assays. K.S. made the reagents and performed the co-immunoprecipitation experiments. E.M.V. performed and analyzed the pupariation assays. E.M.V., A.P.C., A.M., F.H., and A.M.G. developed *Lgr4* transgenes and performed qPCR assays. P. Schlegel and M.J.P. performed the connectome reconstruction and analyses. C.-H.Y. and I.M.-A. developed the critical reagents. J.S.W. contributed to and supervised the behavioral analyses and custom code. A.C. performed and supervised the connectome reconstruction. P. Soba made the reagents, contributed to the circuit and behavioral analyses, supervised the work, and wrote the manuscript.

DECLARATION OF INTERESTS

The authors declare no competing interests.

Received: February 12, 2021
Revised: October 5, 2021
Accepted: October 29, 2021
Published: November 18, 2021

REFERENCES

1. Branco, T., and Redgrave, P. (2020). The neural basis of escape behavior in vertebrates. *Annu. Rev. Neurosci.* **43**, 417–439.
2. Im, S.H., and Galko, M.J. (2012). Pokes, sunburn, and hot sauce: *Drosophila* as an emerging model for the biology of nociception. *Dev. Dyn.* **241**, 16–26.
3. Hesselson, D., Walker, D.S., Massingham, J.N., Schafer, W.R., Neely, G.G., and Chew, Y.L. (2020). Invertebrate models of nociception. In *The Oxford Handbook of the Neurobiology of Pain*, J.N. Wood, ed. (Oxford University Press), pp. 60–100.
4. Basbaum, A.I., Bautista, D.M., Scherrer, G., and Julius, D. (2009). Cellular and molecular mechanisms of pain. *Cell* **139**, 267–284.
5. Chatzigeorgiou, M., Yoo, S., Watson, J.D., Lee, W.H., Spencer, W.C., Kindt, K.S., Hwang, S.W., Miller, D.M., 3rd, Treinin, M., Driscoll, M., and Schafer, W.R. (2010). Specific roles for DEG/ENaC and TRP channels in touch and thermosensation in *C. elegans* nociceptors. *Nat. Neurosci.* **13**, 861–868.
6. Tracey, W.D., Jr., Wilson, R.I., Laurent, G., and Benzer, S. (2003). painless, a *Drosophila* gene essential for nociception. *Cell* **113**, 261–273.
7. Julius, D. (2013). TRP channels and pain. *Annu. Rev. Cell Dev. Biol.* **29**, 355–384.
8. Barik, A., Thompson, J.H., Seltzer, M., Ghitani, N., and Chesler, A.T. (2018). A brainstem-spinal circuit controlling nociceptive behavior. *Neuron* **100**, 1491–1503.e3.
9. Tovote, P., Esposito, M.S., Botta, P., Chaudun, F., Fadok, J.P., Markovic, M., Wolff, S.B.E., Ramakrishnan, C., Fenno, L., Deisseroth, K., et al. (2016). Midbrain circuits for defensive behaviour. *Nature* **534**, 206–212.
10. Fadok, J.P., Krabbe, S., Markovic, M., Courtin, J., Xu, C., Massi, L., Botta, P., Bylund, K., Müller, C., Kovacevic, A., et al. (2017). A competitive inhibitory circuit for selection of active and passive fear responses. *Nature* **542**, 96–100.
11. Dunn, T.W., Gebhardt, C., Naumann, E.A., Riegler, C., Ahrens, M.B., Engert, F., and Del Bene, F. (2016). Neural circuits underlying visually evoked escapes in larval zebrafish. *Neuron* **89**, 613–628.
12. Kupfermann, I., Castellucci, V., Pinsker, H., and Kandel, E. (1970). Neuronal correlates of habituation and dishabituation of the gill-withdrawal reflex in *Aplysia*. *Science* **167**, 1743–1745.
13. Bezares-Calderón, L.A., Berger, J., Jasek, S., Verasztó, C., Mendes, S., Gühmann, M., Almeda, R., Shahidi, R., and Jékely, G. (2018). Neural circuitry of a polycystin-mediated hydrodynamic startle response for predator avoidance. *eLife* **7**, 1–28.
14. Ohyama, T., Schneider-Mizell, C.M., Fetter, R.D., Aleman, J.V., Franconville, R., Rivera-Alba, M., Mensh, B.D., Branson, K.M., Simpson, J.H., Truman, J.W., et al. (2015). A multilevel multimodal circuit enhances action selection in *Drosophila*. *Nature* **520**, 633–639.
15. Jovanic, T., Schneider-Mizell, C.M., Shao, M., Masson, J.-B., Denisov, G., Fetter, R.D., Mensh, B.D., Truman, J.W., Cardona, A., and Zlatić, M. (2016). Competitive disinhibition mediates behavioral choice and sequences in *Drosophila*. *Cell* **167**, 858–870.e19.
16. Abraira, V.E., and Ginty, D.D. (2013). The sensory neurons of touch. *Neuron* **79**, 618–639.
17. Koch, S.C., Acton, D., and Goulding, M. (2018). Spinal circuits for touch, pain, and itch. *Annu. Rev. Physiol.* **80**, 189–217.
18. Kaupp, U.B. (2010). Olfactory signalling in vertebrates and insects: differences and commonalities. *Nat. Rev. Neurosci.* **11**, 188–200.
19. Haverkamp, A., Hansson, B.S., and Knaden, M. (2018). Combinatorial codes and labeled lines: how insects use olfactory cues to find and judge

- food, mates, and oviposition sites in complex environments. *Front. Physiol.* **9**, 49.
20. van den Pol, A.N. (2012). Neuropeptide transmission in brain circuits. *Neuron* **76**, 98–115.
21. Taghert, P.H., and Nitabach, M.N. (2012). Peptide neuromodulation in invertebrate model systems. *Neuron* **76**, 82–97.
22. Bargmann, C.I., and Marder, E. (2013). From the connectome to brain function. *Nat. Methods* **10**, 483–490.
23. Jékely, G., Melzer, S., Beets, I., Kadow, I.C.G., Koene, J., Haddad, S., and Holden-Dye, L. (2018). The long and the short of it - a perspective on peptidergic regulation of circuits and behaviour. *J. Exp. Biol.* **221**, jeb166710.
24. Schlegel, P., Texada, M.J., Miroshnikow, A., Schoofs, A., Hückesfeld, S., Peters, M., Schneider-Mizell, C.M., Lacin, H., Li, F., Fetter, R.D., et al. (2016). Synaptic transmission parallels neuromodulation in a central food-intake circuit. *eLife* **5**, 462–465.
25. Shakiryanova, D., Tully, A., Hewes, R.S., Deitcher, D.L., and Levitan, E.S. (2005). Activity-dependent liberation of synaptic neuropeptide vesicles. *Nat. Neurosci.* **8**, 173–178.
26. Nässel, D.R. (2009). Neuropeptide signaling near and far: how localized and timed is the action of neuropeptides in brain circuits? *Invert. Neurosci.* **9**, 57–75.
27. Nusbaum, M.P., Blitz, D.M., and Marder, E. (2017). Functional consequences of neuropeptide and small-molecule co-transmission. *Nat. Rev. Neurosci.* **18**, 389–403.
28. Gerhard, S., Andrade, I., Fetter, R.D., Cardona, A., and Schneider-Mizell, C.M. (2017). Conserved neural circuit structure across *Drosophila* larval development revealed by comparative connectomics. *eLife* **6**, 1–17.
29. Schneider-Mizell, C.M., Gerhard, S., Longair, M., Kazimiers, T., Li, F., Zwart, M.F., Champion, A., Midgley, F.M., Fetter, R.D., Saalfeld, S., and Cardona, A. (2016). Quantitative neuroanatomy for connectomics in *Drosophila*. *eLife* **5**, 1133–1145.
30. Hu, C., Petersen, M., Hoyer, N., Spitzweck, B., Tenedini, F., Wang, D., Gruschka, A., Burchardt, L.S., Szpotowicz, E., Schweizer, M., et al. (2017). Sensory integration and neuromodulatory feedback facilitate *Drosophila* mechanonociceptive behavior. *Nat. Neurosci.* **20**, 1085–1095.
31. Burgos, A., Honjo, K., Ohyama, T., Qian, C.S., Shin, G.J., Gohl, D.M., Silies, M., Tracey, W.D., Zlatic, M., Cardona, A., and Grueber, W.B. (2018). Nociceptive interneurons control modular motor pathways to promote escape behavior in *Drosophila*. *eLife* **7**, e26016.
32. Takagi, S., Cocanougher, B.T., Niki, S., Miyamoto, D., Kohsaka, H., Kazama, H., Fetter, R.D., Truman, J.W., Zlatic, M., Cardona, A., and Nose, A. (2017). Divergent connectivity of homologous command-like neurons mediates segment-specific touch responses in *Drosophila*. *Neuron* **96**, 1373–1387.e6.
33. Niu, J., Ding, L., Li, J.J., Kim, H., Liu, J., Li, H., Moberly, A., Badea, T.C., Duncan, I.D., Son, Y.-J., et al. (2013). Modality-based organization of ascending somatosensory axons in the direct dorsal column pathway. *J. Neurosci.* **33**, 17691–17709.
34. Osseward, P.J., 2nd, and Pfaff, S.L. (2019). Cell type and circuit modules in the spinal cord. *Curr. Opin. Neurobiol.* **56**, 175–184.
35. Dubin, A.E., and Patapoutian, A. (2010). Nociceptors: the sensors of the pain pathway. *J. Clin. Invest.* **120**, 3760–3772.
36. Yamanaka, N., Romero, N.M., Martin, F.A., Rewitz, K.F., Sun, M.M., O'Connor, M.B., Léopold, P., Connor, M.B.O., Léopold, P., O'Connor, M.B., et al. (2013). Neuroendocrine control of *Drosophila* larval light preference. *Science* **341**, 1113–1116.
37. Xiang, Y., Yuan, Q., Vogt, N., Looger, L.L., Jan, L.Y., and Jan, Y.N. (2010). Light-avoidance-mediating photoreceptors tile the *Drosophila* larval body wall. *Nature* **468**, 921–926.
38. Sprecher, S.G., Cardona, A., and Hartenstein, V. (2011). The *Drosophila* larval visual system: high-resolution analysis of a simple visual neuropil. *Dev. Biol.* **358**, 33–43.
39. Miguel-Aliaga, I., Thor, S., and Gould, A.P. (2008). Postmitotic specification of *Drosophila* insulinergic neurons from pioneer neurons. *PLoS Biol.* **6**, e58.
40. Mazzoni, E.O., Desplan, C., and Blau, J. (2005). Circadian pacemaker neurons transmit and modulate visual information to control a rapid behavioral response. *Neuron* **45**, 293–300.
41. Dana, H., Sun, Y., Mohar, B., Hulse, B.K., Kerlin, A.M., Hasseman, J.P., Tsegaye, G., Tsang, A., Wong, A., Patel, R., et al. (2019). High-performance calcium sensors for imaging activity in neuronal populations and microcompartments. *Nat. Methods* **16**, 649–657.
42. Linneweber, G.A., Jacobson, J., Busch, K.E., Hudry, B., Christov, C.P., Dormann, D., Yuan, M., Otani, T., Knust, E., de Bono, M., and Miguel-Aliaga, I. (2014). Neuronal control of metabolism through nutrient-dependent modulation of tracheal branching. *Cell* **156**, 69–83.
43. Nicolaï, L.J., Ramaekers, A., Raemaekers, T., Drozdzecki, A., Mauss, A.S., Yan, J., Landgraf, M., Annaert, W., and Hassan, B.A. (2010). Genetically encoded dendritic marker sheds light on neuronal connectivity in *Drosophila*. *Proc. Natl. Acad. Sci. USA* **107**, 20553–20558.
44. Qian, C.S., Kaplow, M., Lee, J.K., and Grueber, W.B. (2018). Diversity of internal sensory neuron axon projection patterns is controlled by the POU-domain protein Pdm3 in *Drosophila* larvae. *J. Neurosci.* **38**, 2081–2093.
45. Kaneko, T., Macara, A.M., Li, R., Hu, Y., Iwasaki, K., Dunning, Z., Firestone, E., Horvatic, S., Guntur, A., Shafer, O.T., et al. (2017). Serotonergic modulation enables pathway-specific plasticity in a developing sensory circuit in *Drosophila*. *Neuron* **95**, 623–638.e4.
46. Macpherson, L.J., Zaharieva, E.E., Kearney, P.J., Alpert, M.H., Lin, T.-Y., Turan, Z., Lee, C.-H., and Gallio, M. (2015). Dynamic labelling of neural connections in multiple colours by trans-synaptic fluorescence complementation. *Nat. Commun.* **6**, 10024.
47. de Haro, M., Al-Ramahi, I., Benito-Sipos, J., López-Arias, B., Dorado, B., Veenstra, J.A., and Herrero, P. (2010). Detailed analysis of leucokinin-expressing neurons and their candidate functions in the *Drosophila* nervous system. *Cell Tissue Res.* **339**, 321–336.
48. Schoofs, A., Hückesfeld, S., Schlegel, P., Miroshnikow, A., Peters, M., Zeymer, M., Spieß, R., Chiang, A.-S., and Pankratz, M.J. (2014). Selection of motor programs for suppressing food intake and inducing locomotion in the *Drosophila* brain. *PLoS Biol.* **12**, e1001893.
49. Dana, H., Mohar, B., Sun, Y., Narayan, S., Gordus, A., Jeremy, P., Tsegaye, G., Holt, G.T., Hu, A., Walpita, D., et al. (2016). Sensitive red protein calcium indicators for imaging neural activity. *eLife* **5**, e12727.
50. Ding, K., Han, Y., Seid, T.W., Buser, C., Karigo, T., Zhang, S., Dickman, D.K., and Anderson, D.J. (2019). Imaging neuropeptide release at synapses with a genetically engineered reporter. *eLife* **8**, e46421.
51. Park, D., Li, P., Dani, A., and Taghert, P.H. (2014). Peptidergic cell-specific synaptotagmins in *Drosophila*: localization to dense-core granules and regulation by the bHLH protein DIMMED. *J. Neurosci.* **34**, 13195–13207.
52. Wong, M.Y., Cavolo, S.L., and Levitan, E.S. (2015). Synaptic neuropeptide release by dynamin-dependent partial release from circulating vesicles. *Mol. Biol. Cell* **26**, 2466–2474.
53. Farina, M., van de Bospoort, R., He, E., Persoon, C.M., van Weering, J.R.T., Broeke, J.H., Verhage, M., and Toonen, R.F. (2015). CAPS-1 promotes fusion competence of stationary dense-core vesicles in presynaptic terminals of mammalian neurons. *eLife* **4**, e05438.
54. Renden, R., Berwin, B., Davis, W., Ann, K., Chin, C.-T., Kreber, R., Ganetzky, B., Martin, T.F.J., and Broadie, K. (2001). *Drosophila* CAPS is an essential gene that regulates dense-core vesicle release and synaptic vesicle fusion. *Neuron* **31**, 421–437.
55. Gontijo, A.M., and Garelli, A. (2018). The biology and evolution of the Dilp8-Lgr3 pathway: a relaxin-like pathway coupling tissue growth and developmental timing control. *Mech. Dev.* **154**, 44–50.
56. Veenstra, J.A., Rombauts, S., and Grbić, M. (2012). In silico cloning of genes encoding neuropeptides, neurohormones and their putative

- G-protein coupled receptors in a spider mite. *Insect Biochem. Mol. Biol.* **42**, 277–295.
57. Deng, B., Li, Q., Liu, X., Cao, Y., Li, B., Qian, Y., Xu, R., Mao, R., Zhou, E., Zhang, W., et al. (2019). Chemoconnectomics: mapping chemical transmission in *Drosophila*. *Neuron* **101**, 876–893.e4.
58. Hori, M., Shibuya, K., Sato, M., and Saito, Y. (2014). Lethal effects of short-wavelength visible light on insects. *Sci. Rep.* **4**, 7383.
59. Shibuya, K., Onodera, S., and Hori, M. (2018). Toxic wavelength of blue light changes as insects grow. *PLoS ONE* **13**, e0199266.
60. Gong, J., Yuan, Y., Ward, A., Kang, L., Zhang, B., Wu, Z., Peng, J., Feng, Z., Liu, J., and Xu, X.Z.S. (2016). The *C. elegans* taste receptor homolog LITE-1 is a photoreceptor. *Cell* **167**, 1252–1263.e10.
61. Guntur, A.R., Gu, P., Takle, K., Chen, J., Xiang, Y., and Yang, C.-H. (2015). *Drosophila* TRPA1 isoforms detect UV light via photochemical production of H₂O₂. *Proc. Natl. Acad. Sci. USA* **112**, E5753–E5761.
62. Lazopulo, S., Lazopulo, A., Baker, J.D., and Syed, S. (2019). Daytime colour preference in *Drosophila* depends on the circadian clock and TRP channels. *Nature* **574**, 108–111.
63. Omamiyuda-Ishikawa, N., Sakai, M., and Emoto, K. (2020). A pair of ascending neurons in the subesophageal zone mediates aversive sensory inputs-evoked backward locomotion in *Drosophila* larvae. *PLoS Genet.* **16**, e1009120.
64. Keene, A.C., Mazzoni, E.O., Zhen, J., Younger, M.A., Yamaguchi, S., Blau, J., Desplan, C., and Sprecher, S.G. (2011). Distinct visual pathways mediate *Drosophila* larval light avoidance and circadian clock entrainment. *J. Neurosci.* **31**, 6527–6534.
65. Hu, Y., Wang, C., Yang, L., Pan, G., Liu, H., Yu, G., and Ye, B. (2020). A neural basis for categorizing sensory stimuli to enhance decision accuracy. *Curr. Biol.* **30**, 4896–4909.e6.
66. Zandawala, M., Marley, R., Davies, S.A., and Nässel, D.R. (2018). Characterization of a set of abdominal neuroendocrine cells that regulate stress physiology using colocalized diuretic peptides in *Drosophila*. *Cell. Mol. Life Sci.* **75**, 1099–1115.
67. Zandawala, M., Yurgel, M.E., Texada, M.J., Liao, S., Rewitz, K.F., Keene, A.C., and Nässel, D.R. (2018). Modulation of *Drosophila* post-feeding physiology and behavior by the neuropeptide leucokinin. *PLoS Genet.* **14**, e1007767.
68. Okusawa, S., Kohsaka, H., and Nose, A. (2014). Serotonin and downstream leucokinin neurons modulate larval turning behavior in *Drosophila*. *J. Neurosci.* **34**, 2544–2558.
69. Grueber, W.B., Jan, L.Y., and Jan, Y.N. (2002). Tiling of the *Drosophila* epidermis by multidendritic sensory neurons. *Development* **129**, 2867–2878.
70. Miroschnikow, A., Schlegel, P., Schoofs, A., Hueckesfeld, S., Li, F., Schneider-Mizell, C.M., Fetter, R.D., Truman, J.W., Cardona, A., and Pankratz, M.J. (2018). Convergence of monosynaptic and polysynaptic sensory paths onto common motor outputs in a *Drosophila* feeding connectome. *eLife* **7**, 1–23.
71. Swanson, L.W., and Lichtman, J.W. (2016). From Cajal to connectome and beyond. *Annu. Rev. Neurosci.* **39**, 197–216.
72. Chen, C., Itakura, E., Nelson, G.M., Sheng, M., Laurent, P., Fenk, L.A., Butcher, R.A., Hegde, R.S., and de Bono, M. (2017). IL-17 is a neuromodulator of *Caenorhabditis elegans* sensory responses. *Nature* **542**, 43–48.
73. Macosko, E.Z., Pokala, N., Feinberg, E.H., Chalasani, S.H., Butcher, R.A., Clardy, J., and Bargmann, C.I. (2009). A hub-and-spoke circuit drives pheromone attraction and social behaviour in *C. elegans*. *Nature* **458**, 1171–1175.
74. Duan, B., Cheng, L., Bourane, S., Britz, O., Padilla, C., Garcia-Campany, L., Krashes, M., Knowlton, W., Velasquez, T., Ren, X., et al. (2014). Identification of spinal circuits transmitting and gating mechanical pain. *Cell* **159**, 1417–1432.
75. Bentley, B., Branicky, R., Barnes, C.L., Chew, Y.L., Yemini, E., Bullmore, E.T., Vértes, P.E., and Schafer, W.R. (2016). The multilayer connectome of *Caenorhabditis elegans*. *PLoS Comput. Biol.* **12**, e1005283.
76. Knobloch, H.S., Charlet, A., Hoffmann, L.C., Eliava, M., Khurlev, S., Cetin, A.H., Osten, P., Schwarz, M.K., Seeburg, P.H., Stoop, R., and Grinevich, V. (2012). Evoked axonal oxytocin release in the central amygdala attenuates fear response. *Neuron* **73**, 553–566.
77. Viviani, D., Charlet, A., Van Den Burg, E., Robinet, C., Hurni, N., Abatis, M., Magara, F., and Stoop, R. (2011). Oxytocin selectively gates fear responses through distinct outputs from the central amygdala. *Science* **333**, 104–107.
78. Hwang, R.Y., Zhong, L., Xu, Y., Johnson, T., Zhang, F., Deisseroth, K., and Tracey, W.D. (2007). Nociceptive neurons protect *Drosophila* larvae from parasitoid wasps. *Curr. Biol.* **17**, 2105–2116.
79. Wietek, J., Rodriguez-Rozada, S., Tutas, J., Tenedini, F., Grimm, C., Oertner, T.G., Soba, P., Hegemann, P., and Wiegert, J.S. (2017). Anion-conducting channelrhodopsins with tuned spectra and modified kinetics engineered for optogenetic manipulation of behavior. *Sci. Rep.* **7**, 14957.
80. Tao, L., Porto, D., Li, Z., Fechner, S., Lee, S.A., Goodman, M.B., Xu, X.Z.S., Lu, H., and Shen, K. (2019). Parallel processing of two mechano-sensory modalities by a single neuron in *C. elegans*. *Dev. Cell* **51**, 617–631.e3.
81. Cohn, R., Morante, I., and Ruta, V. (2015). Coordinated and compartmentalized neuromodulation shapes sensory processing in *Drosophila*. *Cell* **163**, 1742–1755.
82. Boto, T., Louis, T., Jindachomthong, K., Jalink, K., and Tomchik, S.M. (2014). Dopaminergic modulation of cAMP drives nonlinear plasticity across the *Drosophila* mushroom body lobes. *Curr. Biol.* **24**, 822–831.
83. Bilz, F., Geurten, B.R.H., Hancock, C.E., Widmann, A., and Fiala, A. (2020). Visualization of a distributed synaptic memory code in the *Drosophila* brain. *Neuron* **106**, 963–976.e4.
84. Tsubouchi, A., Yano, T., Yokoyama, T.K., Murtin, C., Otsuna, H., and Ito, K. (2017). Topological and modality-specific representation of somatosensory information in the fly brain. *Science* **358**, 615–623.
85. Choi, S., Hachisuka, J., Brett, M.A., Magee, A.R., Omori, Y., Iqbal, N.U., Zhang, D., DeLisle, M.M., Wolfson, R.L., Bai, L., et al. (2020). Parallel ascending spinal pathways for affective touch and pain. *Nature* **587**, 258–263.
86. Branco, T., and Häusser, M. (2010). The single dendritic branch as a fundamental functional unit in the nervous system. *Curr. Opin. Neurobiol.* **20**, 494–502.
87. Euler, T., Detwiler, P.B., and Denk, W. (2002). Directionally selective calcium signals in dendrites of starburst amacrine cells. *Nature* **418**, 845–852.
88. Woods, I.G., Schoppik, D., Shi, V.J., Zimmerman, S., Coleman, H.A., Greenwood, J., Soucy, E.R., and Schier, A.F. (2014). Neuropeptidergic signaling partitions arousal behaviors in zebrafish. *J. Neurosci.* **34**, 3142–3160.
89. Hökfelt, T., Barde, S., Xu, Z.D., Kuteeva, E., Rüegg, J., Le Maitre, E., Risling, M., Kehr, J., Ihnatko, R., Theodorsson, E., et al. (2018). Neuropeptide and small transmitter coexistence: fundamental studies and relevance to mental illness. *Front. Neural Circuits* **12**, 106.
90. Persoon, C.M., Hoogstraaten, R.I., Nassal, J.P., van Weering, J.R.T., Kaeser, P.S., Toonen, R.F., and Verhage, M. (2019). The RAB3-RIM pathway is essential for the release of neuromodulators. *Neuron* **104**, 1065–1080.e12.
91. Duggan, A.W., Morton, C.R., Zhao, Z.Q., and Hendry, I.A. (1987). Noxious heating of the skin releases immunoreactive substance P in the substantia gelatinosa of the cat: a study with antibody microprobes. *Brain Res.* **403**, 345–349.
92. Jan, L.Y., and Jan, Y.N. (1982). Peptidergic transmission in sympathetic ganglia of the frog. *J. Physiol.* **327**, 219–246.

93. Fields, H. (2004). State-dependent opioid control of pain. *Nat. Rev. Neurosci.* *5*, 565–575.
94. Nichols, A.L.A., Eichler, T., Latham, R., and Zimmer, M. (2017). A global brain state underlies *C. elegans* sleep behavior. *Science* *356*, eaam6851.
95. Flavell, S.W., Pokala, N., Macosko, E.Z., Albrecht, D.R., Larsch, J., and Bargmann, C.I. (2013). Serotonin and the neuropeptide PDF initiate and extend opposing behavioral states in *C. elegans*. *Cell* *154*, 1023–1035.
96. Garelli, A., Heredia, F., Casimiro, A.P., Macedo, A., Nunes, C., Garcez, M., Dias, A.R.M., Volonte, Y.A., Uhlmann, T., Caparros, E., et al. (2015). Dilp8 requires the neuronal relaxin receptor Lgr3 to couple growth to developmental timing. *Nat. Commun.* *6*, 8732.
97. Vallejo, D.M., Juarez-Carreño, S., Bolivar, J., Morante, J., and Dominguez, M. (2015). A brain circuit that synchronizes growth and maturation revealed through Dilp8 binding to Lgr3. *Science* *350*, aac6767.
98. Bathgate, R.A.D., Halls, M.L., van der Westhuizen, E.T., Callander, G.E., Kocan, M., and Summers, R.J. (2013). Relaxin family peptides and their receptors. *Physiol. Rev.* *93*, 405–480.
99. Jaszczak, J.S., Wolpe, J.B., Bhandari, R., Jaszczak, R.G., and Halme, A. (2016). Growth coordination during *Drosophila melanogaster* imaginal disc regeneration is mediated by signaling through the relaxin receptor Lgr3 in the prothoracic gland. *Genetics* *204*, 703–709.
100. Colombani, J., Andersen, D.S., Boulan, L., Boone, E., Romero, N., Virolle, V., Texada, M., and Léopold, P. (2015). *Drosophila* Lgr3 couples organ growth with maturation and ensures developmental stability. *Curr. Biol.* *25*, 2723–2729.
101. Kania, A., Gugula, A., Grabowiecka, A., de Ávila, C., Blasiak, T., Rajfur, Z., Lewandowski, M.H., Hess, G., Timofeeva, E., Gundlach, A.L., and Blasiak, A. (2017). Inhibition of oxytocin and vasopressin neuron activity in rat hypothalamic paraventricular nucleus by relaxin-3-RXFP3 signaling. *J. Physiol.* *595*, 3425–3447.
102. Smith, S.J., Sümbül, U., Graybuck, L.T., Collman, F., Seshamani, S., Gala, R., Gilko, O., Elabbady, L., Miller, J.A., Bakken, T.E., et al. (2019). Single-cell transcriptomic evidence for dense intracortical neuropeptide networks. *eLife* *8*, 1–35.
103. Yang, C.-H., Belawat, P., Hafen, E., Jan, L.Y., and Jan, Y.-N. (2008). *Drosophila* egg-laying site selection as a system to study simple decision-making processes. *Science* *319*, 1679–1683.
104. Grönke, S., Clarke, D.-F., Broughton, S., Andrews, T.D., and Partridge, L. (2010). Molecular evolution and functional characterization of *Drosophila* insulin-like peptides. *PLoS Genet.* *6*, e1000857.
105. Karupudurai, T., Lin, T.-Y., Ting, C.-Y., Pursley, R., Melnattur, K.V., Diao, F., White, B.H., Macpherson, L.J., Gallio, M., Pohida, T., and Lee, C.H. (2014). A hard-wired glutamatergic circuit pools and relays UV signals to mediate spectral preference in *Drosophila*. *Neuron* *81*, 603–615.
106. Baines, R.A., Uhler, J.P., Thompson, A., Sweeney, S.T., and Bate, M. (2001). Altered electrical properties in *Drosophila* neurons developing without synaptic transmission. *J. Neurosci.* *21*, 1523–1531.
107. Watanabe, K., Chiu, H., Pfeiffer, B.D., Wong, A.M., Hooper, E.D., Rubin, G.M., and Anderson, D.J. (2017). A circuit node that integrates convergent input from neuromodulatory and social behavior-promoting neurons to control aggression in *Drosophila*. *Neuron* *95*, 1112–1128.e7.
108. Sancer, G., Kind, E., Plazaola-Sasieta, H., Balke, J., Pham, T., Hasan, A., Münch, L.O., Courgeon, M., Mathejczyk, T.F., and Wernet, M.F. (2019). Modality-specific circuits for skylight orientation in the fly visual system. *Curr. Biol.* *29*, 2812–2825.e4.
109. Saalfeld, S., Cardona, A., Hartenstein, V., and Tomancak, P. (2009). CATMAID: collaborative annotation toolkit for massive amounts of image data. *Bioinformatics* *25*, 1984–1986.
110. Thévenaz, P., Ruttimann, U.E., and Unser, M. (1998). A pyramid approach to subpixel registration based on intensity. *IEEE Trans. Image Process.* *7*, 27–41.
111. Risse, B., Thomas, S., Otto, N., Löpmeier, T., Valkov, D., Jiang, X., and Klämbt, C. (2013). FIM, a novel FTIR-based imaging method for high throughput locomotion analysis. *PLoS ONE* *8*, e53963.
112. Groth, A.C., Fish, M., Nusse, R., and Calos, M.P. (2004). Construction of transgenic *Drosophila* by using the site-specific integrase from phage phiC31. *Genetics* *166*, 1775–1782.
113. Tenedini, F.M., Sáez González, M., Hu, C., Pedersen, L.H., Petrucci, M.M., Spitzweck, B., Wang, D., Richter, M., Petersen, M., Szpotowicz, E., et al. (2019). Maintenance of cell type-specific connectivity and circuit function requires Tao kinase. *Nat. Commun.* *10*, 3506.
114. Ingles-Prieto, A., Furthmann, N., Crossman, S.H., Tichy, A.-M., Hoyer, N., Petersen, M., Zheden, V., Biebl, J., Reichhart, E., Gyoergy, A., et al. (2021). Optogenetic delivery of trophic signals in a genetic model of Parkinson's disease. *PLoS Genet.* *17*, e1009479.
115. Hoyer, N., Petersen, M., Tenedini, F., and Soba, P. (2018). Assaying mechanonociceptive behavior in *Drosophila* larvae. *Bio Protoc.* *8*, e2736.
116. Soba, P., Han, C., Zheng, Y., Perea, D., Miguel-Aliaga, I., Jan, L.Y., and Jan, Y.N. (2015). The Ret receptor regulates sensory neuron dendrite growth and integrin mediated adhesion. *eLife* *4*, e05491.

STAR★METHODS

KEY RESOURCES TABLE

| REAGENT or RESOURCE | SOURCE | IDENTIFIER |
|---|---|---|
| Antibodies | | |
| Rabbit polyclonal anti-IIP7 | ³⁹ | N/A |
| Rabbit polyclonal anti-Leucokinin | Dr. Dick Nässel, Stockholm University, Sweden | N/A |
| Chicken polyclonal anti-GFP | Abcam | Cat# ab13970; RRID: AB_300798 |
| Rat monoclonal anti-HA | Roche | Cat# ROAHAHA; RRID: AB_2687407 |
| Mouse monoclonal anti-Fas2 (1D4) | DSHB | RRID: AB_528235 |
| Mouse monoclonal anti-myc (9E10) | Sigma-Aldrich | Cat# M4439; RRID: AB_439694 |
| Mouse monoclonal anti-Flag M2 | Sigma-Aldrich | Cat# P2983; RRID: AB_439685 |
| Alexa Fluor 488 Donkey anti-mouse | Jackson ImmunoResearch | Cat# 715-545-150; RRID: AB_2340846 |
| Cy3 polyclonal Goat anti-Rabbit | Jackson ImmunoResearch | Cat# 111-165-003; RRID: AB_2338000 |
| Cy5 polyclonal Donkey anti-Chicken | Jackson ImmunoResearch | Cat# 703-175-155; RRID: AB_2340365 |
| Dylight 649 monoclonal mouse anti-Rabbit | Jackson immunoResearch | Cat# 211-492-171; RRID: AB_2339164 |
| Chemicals, peptides, and recombinant proteins | | |
| All-trans Retinal | Sigma-Aldrich | Cat# R2500 |
| Schneider's <i>Drosophila</i> medium | Thermo-Fisher | Cat# 21720024 |
| Ethyl butyrate | Sigma-Aldrich | Cat# E15701 |
| Critical commercial assays | | |
| High Pure RNA Tissue Kit | Roche | Cat# 12033674001 |
| Maxima First Strand cDNA Synthesis Kit for RT-quantitative PCR | Thermo Scientific | Cat# K1641 |
| High Pure PCR template preparation kit | Roche | Cat# 11796828001 |
| Deposited data | | |
| Catmaid neuronal reconstructions | This paper | https://11em.catmaid.virtuallyflybrain.org/?pid=1 |
| Experimental models: Cell lines | | |
| <i>D. melanogaster</i> : Cell line S2: S2-DRSC | DGRC | RRID: CVCL_Z992 |
| Experimental models: Organisms/strains | | |
| <i>D. melanogaster</i> : w ¹¹¹⁸ | Bloomington <i>Drosophila</i> Stock Center | BDSC:3605 |
| <i>D. melanogaster</i> : w[1118]; P{y[+t7.7] w[+mC] = GMR35B01-GAL4}attP2 | Bloomington <i>Drosophila</i> Stock Center | BDSC: 49898 |
| <i>D. melanogaster</i> : w[1118]; P{y[+t7.7] w[+mC] = GMR73B01-GAL4}attP2 | Bloomington <i>Drosophila</i> Stock Center | BDSC: 39809 |
| <i>D. melanogaster</i> : w[*]; wg[Sp-1]/CyO; P{w[+mC] = Gr28b.c-GAL4.6.5}3 | Bloomington <i>Drosophila</i> Stock Center | BDSC: 57619 |
| <i>D. melanogaster</i> : w[*]; P{w[+mC] = Gr89a-GAL4.2}11/CyO | Bloomington <i>Drosophila</i> Stock Center | BDSC: 57676 |
| <i>D. melanogaster</i> : w[1118]; P{y[+t7.7] w[+mC] = GMR22C07-GAL4}attP2 | Bloomington <i>Drosophila</i> Stock Center | BDSC: 48975 |
| <i>D. melanogaster</i> : w[1118]; P{y[+t7.7] w[+mC] = GMR27H06-lexA}attP40 | Bloomington <i>Drosophila</i> Stock Center | BDSC: 54751 |
| <i>D. melanogaster</i> : w[1118]; P{y[+t7.7] w[+mC] = 20XUAS-IVS-GCaMP6s}attP40 | Bloomington <i>Drosophila</i> Stock Center | BDSC: 42746 |
| <i>D. melanogaster</i> : w1118; P{20XUAS-IVS-GCaMP6m}attP40 | Bloomington <i>Drosophila</i> Stock Center | BDSC: 42748 |

(Continued on next page)

Continued

| REAGENT or RESOURCE | SOURCE | IDENTIFIER |
|--|---|-------------|
| <i>D. melanogaster</i> : w[1118]; P{y[+t7.7] w[+mC]} = 20XUAS-IVS-jGCaMP7s}VK00005 | Bloomington Drosophila Stock Center | BDSC: 79032 |
| <i>D. melanogaster</i> : w[1118]; P{y[+t7.7] w[+mC]} = 20XUAS-IVS-CsChrimson.mVenus}attP2 | Bloomington Drosophila Stock Center | BDSC: 55136 |
| <i>D. melanogaster</i> : w[1118]; P{y[+t7.7] w[+mC]} = 13XLexAop2-IVS-CsChrimson.mVenus}attP2 | Bloomington Drosophila Stock Center | BDSC: 55139 |
| <i>D. melanogaster</i> : w[*]; PBac{y[+mDint2] w[+mC]} = 20XUAS-IVS-NES-jRCaMP1b-p10}VK00005 | Bloomington Drosophila Stock Center | BDSC: 63793 |
| <i>D. melanogaster</i> : P{w[+mC]} = GMR-hid}G1/CyO, P{ry[+t7.2]} = sevRas1.V12}FK1 | Bloomington Drosophila Stock Center | BDSC: 5771 |
| <i>D. melanogaster</i> : w[1118]; PBac{y[+mDint2] w[+mC]} = UAS-CD4-tdGFP}VK00033 | Bloomington Drosophila Stock Center | BDSC: 35836 |
| <i>D. melanogaster</i> : y[1] w[*] Mi{Trojan-GAL4.1}Lgr4{MI06794-TG4.1} | Bloomington Drosophila Stock Center | BDSC: 77775 |
| <i>D. melanogaster</i> : w* Tl{TI}Lgr4attP (Lgr4 ^{ko}) | Bloomington Drosophila Stock Center | BDSC: 84478 |
| <i>D. melanogaster</i> : w[1118]; PBac{y[+mDint2] w[+mC]} = UAS-CD4-tdTom}VK00033 | Bloomington Drosophila Stock Center | BDSC: 35837 |
| <i>D. melanogaster</i> : w[1118]; PBac{y[+mDint2] w[+mC]} = UAS-CD4-tdGFP}VK00033 | Bloomington Drosophila Stock Center | BDSC: 35836 |
| <i>D. melanogaster</i> : w[1118]; P{w[+mC]} = UAS-DenMark}3 | Bloomington Drosophila Stock Center | BDSC: 33061 |
| <i>D. melanogaster</i> : w[*]; P{w[+mC]} = lexAop-nSyb-spGFP1-10}2, P{w[+mC]} = UAS-CD4-spGFP11}2; MKRS/TM6B (Syb-GRASP) | Bloomington Drosophila Stock Center | BDSC: 64315 |
| <i>D. melanogaster</i> : w[*]; wg[Sp-1]/CyO; P{w[+mC]} = tubP(FRT.stop)GAL80}3 | Bloomington Drosophila Stock Center | BDSC: 39213 |
| <i>D. melanogaster</i> : UAS-spGFP1-10-Syb | M. Gallio, Northwestern University, Evanston, USA | N/A |
| <i>D. melanogaster</i> : UAS-Sytα-myc | 51 | N/A |
| <i>D. melanogaster</i> : w*;tsh-Gal80/CyO | J. Simpson, UCSB, Santa Barbara, USA | N/A |
| <i>D. melanogaster</i> : LexAop-CD4-sp11-CD4-tdTomato | 30 | N/A |
| <i>D. melanogaster</i> : A08n-Gal4 (82E12-Gal4AD, 6.14.3-Gal4DBD) | 30 | N/A |
| <i>D. melanogaster</i> : Dp7(4-3)-LexA | 30 | N/A |
| <i>D. melanogaster</i> : sNPF ^{C00448} | 30 | N/A |
| <i>D. melanogaster</i> : sNPF ^{MI01807} | 30 | N/A |
| <i>D. melanogaster</i> : llp7-LexA | 103 | N/A |
| <i>D. melanogaster</i> : llp7 ^{ko} | 104 | N/A |
| <i>D. melanogaster</i> : w[1118]; LexAop-Kir2.1 | 30 | N/A |
| <i>D. melanogaster</i> : w[1118]; LexAop-TnT-HA | 105 | N/A |
| <i>D. melanogaster</i> : Hugin ^{VNC} -Gal4 | 48 | N/A |
| <i>D. melanogaster</i> : UAS-Kir2.1 | 106 | N/A |
| <i>D. melanogaster</i> : Otd-Flp | 107 | N/A |
| <i>D. melanogaster</i> : Dp7(4-3)-Gal4 | This paper | N/A |
| <i>D. melanogaster</i> : UAS-NPRR ^{lp7} | This paper | N/A |
| <i>D. melanogaster</i> : UAS-llp7 | This paper | N/A |
| <i>D. melanogaster</i> : UAS-Lgr4-HA-flag | This paper | N/A |

(Continued on next page)

Continued

| REAGENT or RESOURCE | SOURCE | IDENTIFIER |
|---|--|---|
| <i>D. melanogaster</i> : <i>Lk-Gal4</i> | ⁴⁷ | N/A |
| <i>D. melanogaster</i> : <i>GMR-LexA</i> | ¹⁰⁸ | N/A |
| <i>D. melanogaster</i> : <i>UAS-Cadps-RNAi</i> | Vienna <i>Drosophila</i> Stock Center | VDRC: KK110055 |
| Oligonucleotides | | |
| Primers for HA-tagged <i>Ilp7</i> and <i>Lgr4</i> cloning, see Table S2 | This paper | N/A |
| Primers for <i>Lgr4</i> qRT-PCR, see Table S2 | This paper | N/A |
| Software and algorithms | | |
| Collaborative annotation toolkit for massive amount of image data (CATMAID) | Janelia research campus, USA, ¹⁰⁹ | RRID: SCR_006278 |
| Ethovision XT-X2 | Noldus Information Technology, Wageningen, Netherlands | RRID: SCR_000441 |
| Pylon Camera Software Suite | Basler, Switzerland | N/A |
| StreamPix 6 | Norpix, Montreal, Quebec, Canada | RRID: SCR_015773 |
| Fiji/ImageJ | NIH, Bethesda | RRID: SCR_002285 |
| Prism | Graphpad, San Diego, CA, USA | RRID: SCR_00279 |
| StackReg, ImageJ plugin | EPFL, Lausanne, Switzerland ¹¹⁰ | N/A |
| Time Series analyzer V3, ImageJ plugin | UCLA, California, USA | RRID: SCR_014269 |
| FimTrack | University of Münster, Germany ¹¹¹ | https://github.com/kostasl/FIMTrack |
| Temporal larval distribution analysis scripts | This paper | https://github.com/formozov/larva_tracking_Imambocus_et_al |
| Other | | |
| CoolLED pE-4000 | CoolLED, Andover, UK | N/A |
| RGB-LED plate | Phlox, Provence, France | N/A |
| Custom incubator with RGB LEDs | ¹¹¹ | N/A |

RESOURCE AVAILABILITY

Lead contact

Further information and requests for resources and reagents should be directed to and will be fulfilled by the Lead Contact, Peter Soba (psoba@uni-bonn.de).

Materials availability

Lines generated and described in this study are available on request from the Lead Contact.

Data and code availability

- All data reported in this paper is available from the lead contact upon request.
- All neurons reconstructed from volume EM were archived in the Virtual Fly Brain server, and are accessible via CATMAID software at this address: <https://l1em.catmaid.virtualflybrain.org/?pid=1>
- Code and scripts used to analyze larval distribution in two choice assays are available at this address: https://github.com/formozov/larva_tracking_Imambocus_et_al
- Any additional information required to reanalyze the data reported in this paper is available from the lead contact upon request.

EXPERIMENTAL MODEL AND SUBJECT DETAILS

Fly stocks

Drosophila melanogaster were reared at 25°C and 70% humidity with a 12 light/dark cycle on standard fly food. Transgenic lines were maintained in either *white* mutant (*w*⁻) or yellow-white (*y*⁻, *w*⁻) backgrounds. For analysis, 3rd instar foraging stage larvae of both sexes were used in this study (94h ± 2h AEL unless stated otherwise). No sex-specific effects were part of this study. For fly line details see [Key resources table](#). Lines were obtained from the Bloomington *Drosophila* Stock Center or the Vienna *Drosophila* Stock Center

unless stated otherwise. *UAS-CsChrimson* was used as an optogenetic actuator to stimulate specific neurons. *UAS-Kir2.1* or *UAS-TNT* were used to block activity/function of specific neurons. Experimental genotypes for quantitative comparisons are listed in [Table S1](#).

S2-DRSC cell line

Drosophila S2-DRSC cells (sex: male) were cultured in Schneider's *Drosophila* medium supplemented with 10% fetal calf serum, glutamine and Penicillin/Streptomycin (ThermoFisher, Carlsbad, CA, USA). Cells were passaged every 3-5 days and maintained in as semi-adherent cultures.

METHOD DETAILS

Generation of plasmids and transgenes

Dp7-Gal4 is a 2nd chromosome insertion and was generated analogously to *Dp7-LexA*³⁰ using a 1,099 bp fragment of the *Ilp7* enhancer region at the 5' end of the *Ilp7* gene (starting from -1,131 to -33, where the ATG for *Ilp7* starts at position 0). The genomic region was amplified by PCR and cloned into pCasper-AUG-GAL4. Transgenes were generated using P-element-mediated transformation. The *UAS-Ilp7* transgene was generated by cloning *Ilp7* cDNA via *EcoRI* into the pUAST vector and P-element mediated transformation. A *UAS-Ilp7* insertion on the 3rd chromosome was used in this study. The *Ilp7* neuropeptide release reporter (NPRR^{Ilp7}) was designed analogously to Ding et al.,⁵⁰ by fusing GCaMP6s to the C terminus of the *Ilp7* neuropeptide. *Ilp7* cDNA was obtained from the *Drosophila* Genetics Resource Center (DGRC) and amplified from clone F118537 by PCR with specific primers carrying *NotI* and *NdeI* restriction sites, and fused in frame with GCaMP6s (Addgene) via *NdeI/XbaI* into the pUAST-*AttB* vector. Transgenes were made by *phiC31*-mediated genomic integration¹¹² into the *AttP2* landing site (BestGene, Chino Hills, CA, USA). HA-tagged *Ilp7* was generated by inserting the HA sequence after the signal peptide sequence at position 34 of the *Ilp7* cDNA using overlap-PCR. Primers containing the HA-tag sequence were used for amplification and cloning into the pUAST-*AttB* vector via *NotI/XhoI*.

Lgr4 cDNA was amplified from DGRC clone UFO07708 (BDGP Tagged ORF collection) by PCR using specific primers and inserted into a pUAST-*AttB* vector containing a C-terminal 3xflag-6xHis-tag via *NotI/XhoI*. The *Lgr4*^{l263A} mutation was introduced using overlap-PCR with specific primers for the codon change and cloned via internal *EcoRI/StuI* sites into the original *Lgr4* cDNA. To remove the Leucine-rich repeats (LRRs), *Lgr4* cDNA was synthesized lacking amino acids 81-426 (*Lgr4*^{Δ81-426}, GeneArt, ThermoFisher) and subcloned into pUAST-*AttB* vector containing a C-terminal 3xflag-6xHis-tag via *NotI/XhoI*. All constructs were verified by sequencing. Primers used for cloning are listed in [Table S2](#).

Transgenic flies carrying *UAS-Lgr4-HA* (pUAST-*Lgr4-CFLAGHA-BD-PHI*, consisting of full length *Lgr4* cDNA dually-tagged with a Flag-HA C-terminal fusion (UFO07708, BDGP Tagged ORF collection)) were made using *phiC31*-mediated genomic integration by injection into *y¹ M{vas-int.Dm}ZH-2A w^{*}; M{3xP3-RFP.attP}ZH-51C* (BestGene, Chino Hills, CA, USA).

Neuronal reconstruction and circuit mapping

Neuronal reconstruction was performed on ssTEM images of the first instar larvae using the web-based software CATMAID.¹⁰⁹ *Dp7* neurons and its partners were manually reconstructed similarly as described^{14,29} and the location of pre- and post-synapses were identified. Synapses were annotated using the following 4 criteria: (1) the presence of a highly visible T-bar, (2) the presence of numerous synaptic vesicles close to the T-bars, (3) contact of pre- and post-synaptic membranes in at least 2 consecutive sections (4) the presence of a synaptic cleft. We then reconstructed the pre- and postsynaptic partners of *Dp7* from the synaptic sites and identified the v'td2 sensory neurons. Neuronal reconstruction validation was done as previously described^{14,29} by using the iterative method. Pre- and post-synaptic illustrations between 2 neurons were extracted using CATMAID's 3D-visualization tools. All reconstructed neurons from the EM volume are accessible via CATMAID software (<https://11em.catmaid.virtualflybrain.org/?pid=1>).

Immunohistochemistry and confocal imaging

Larval brains from genotypes labeling *Dp7* (*Dp7-Gal4*, *Ilp7-LexA*, *Ilp7-Gal4*) or ABLK (*Lk-Gal4*) neurons with a reporter (*LexAop-CD4-spGFP11-tdTomato*, *UAS-CD4-tdGFP*, *UAS-DenMARK*, *UAS-Lgr4-HA*, *UAS-Sytα-myc*) were dissected in PBS, fixed in 4% formaldehyde with PBS for 15 min at room temperature, washed in PBST (PBS with 0.3% Triton X-100 (Roth Karlsruhe, Germany)), incubated with primary antibodies at room temperature overnight, washed in PBST and incubated with corresponding fluorescent dye-coupled secondary antibodies for 1 hour (Cy3, Cy5 or Dylight 649-coupled secondary antibodies, Jackson ImmunoResearch, Ely, UK). Samples were mounted either on poly-L-lysine (Sigma) coated coverslips or on Superfrost slides in Slow Fade Gold (Thermo Fisher, Carlsbad, CA, USA). For anatomical inspection of *Dp7* and ABLK neurons, native reporter fluorescence was sufficiently bright to be visualized together with antibody immunostaining by confocal microscopy (Zeiss LSM700 or LSM900). Primary antibodies used: rabbit anti-*Ilp7* (1:5000), rabbit anti-Lk (1:1000), mouse anti-Fas2 (1:100, DSHB), rat anti-HA (1:100), mouse anti-myc: (1:100). Corresponding fluorescent dye-coupled secondary antibodies were used at 1:300. Confocal Z stacks were processed in Fiji (ImageJ, NIH, Bethesda).

Labeling of synapses between *Dp7* and v'td2 neurons using Syb-GRASP⁴⁶ was performed as described.¹¹³ Larval brains (*UAS-spGFP1-10-Syb*, *LexAop-spGFP11;73B01-Gal4/Ilp7-LexA*) were dissected in 5 mM dissection buffer (108 mM NaCl, 5 mM KCl, 4 mM NaHCO₃, 1 mM NaH₂PO₄, 5 mM Trehalose, 10mM Sucrose, 5 mM HEPES, 8.2 mM MgCl₂, 2 mM CaCl₂, pH 7.4), washed 3 times/5 s alternating between dissection buffer containing 5 mM KCl and 70 mM KCl, respectively, followed by 10 minutes

incubation in 5 mM dissection buffer. Brains were then fixed in 4% formaldehyde/PBS for 15 minutes, followed by immunohistochemistry (rabbit anti-IIP7: 1:5000, chicken anti-GFP: 1:500, corresponding fluorescent dye-coupled secondary antibodies: 1:300) and mounting as described above. Z stacks were obtained using confocal microscopy and processed in Fiji (ImageJ, NIH, Bethesda).

Developmental toxicity assay

Wild-type flies (w^{1118}) were staged for 4 to 6 hours. After 1 day, 50 freshly hatched L1 larvae were transferred to a grape agar Petri dish supplemented with yeast paste. Yeast paste was replaced daily to prevent decay. The larvae were then incubated either under green light ($2.5\mu\text{W}/\text{mm}^2$) or blue light ($2.5\mu\text{W}/\text{mm}^2$) for at least 9 days at 25°C in a custom incubator (described in Ingles-Prieto et al.¹¹⁴). The temperature of the substrate or larvae was measured after 1h, 6h and 16h of blue or green light incubation and remained within the nominal temperature of the incubator ($25.15 \pm 1.75^\circ\text{C}$). After 9 days, the number of eclosed flies and the numbers of dead animals (pharate adults, white pupae, 2nd and 3rd instar larvae, 1st instar or lost upon transfer) were counted. The assay was repeated 5 times for each condition.

Light avoidance assays

After pre-staging, crosses of adult flies with the appropriate genotype were allowed to lay eggs on grape agar plates supplemented with fresh yeast paste within a fixed time frame (Zeitgeber (ZT) 4-6) for 1-3 h depending on the number of fertilized eggs to minimize overcrowding.

Third instar foraging larvae ($94\text{ h} \pm 1.5\text{ h AEL}$) were subjected to a 15 min light avoidance assay as described^{36,40} with modifications. The experimental setup consisted of a dark chamber with a white light source (365-580 nm, intensity $6.9\text{-}3.3\mu\text{W}/\text{mm}^2$ on light side, respectively, $< 0.01\mu\text{W}/\text{mm}^2$ on dark side) illuminating one half of a 10 cm agar plate (12 mL of 2% agar dissolved in ddH₂O (Roth, Karlsruhe, Germany)). An infrared LED source surrounding the plates allowed live recording of larval distribution in darkness with a digital camera (Basler ace-2040 gm, Basler, Switzerland).

For each trial, 20 larvae were preincubated in darkness for 15 min. The animals were placed in the middle of each Petri dish at the light /dark junction. Each trial was run for at least 15 min, recorded by a camera at the top of the chamber using Ethovision XT, Pylon (Basler) or StreamPix 6 (Norpix, Montreal, Canada). For each genotype, typically 10 trials consisting of 20 larvae each were performed. If more than 3 larvae were lost, the trial was excluded.

Mechanonociception assays

Mechanonociception experiments were performed on staged 96h old 3rd instar larvae as described^{30,115} using a calibrated 50 mN *von Frey* filament. Larvae were stimulated on mid-abdominal segments (A3–A5) twice within 2 s and the behavioral response to the 2nd stimulus was scored (no response, stop, or stop and turn as non-nociceptive, bending and rolling as nociceptive). Each genotype was tested multiple times on different days in a blinded fashion.

Locomotion and chemotaxis assays

Larvae were staged on grape juice agar plates and fed with yeast paste. Third instar larvae ($94\text{ h} \pm 2\text{ h}$ after egg laying) were used for all experiments. For locomotion analysis under dark or blue light conditions, animals were carefully transferred to a 2% agar film on a FTIR (frustrated total internal reflection) based tracking system (FIM, University of Münster)¹¹¹ using a Basler ac2040-25 gm camera (Basler, Ahrensburg, Germany). Five freely moving larvae per trial were recorded for 1 min in the dark, or for 1 min with $4.5\mu\text{W}/\text{mm}^2$ 470 nm light illumination from a LED light source (RGB-BL-S-Q-1R, Phlox, Aix-en-Provence, France). Locomotion was tracked with 10 frames per second.

For chemotaxis assays, 10 μl of 125mM Ethyl butyrate (Sigma-Aldrich) diluted in paraffin oil were placed in an odor container on one side of a 10 cm agar plate. Experiments were performed under minimum light conditions as for locomotion assays. Five freely moving larvae per trial were video-captured for 5min.

Optogenetic behavioral assays

Staged third instar larvae ($96\text{ h} \pm 3\text{ h AEL}$) expressing CsChrimson in specific neuronal subsets ($v'td2: 22C07-Gal4$, $73B01-Gal4$, $Gr89a-Gal4$, Lk neuron subsets: $Lk-Gal4$ without or with $tsh-Gal80$ or $otd-Flp$; $tub-FRT-STOP-FRT-Gal80$) were grown in darkness on grape agar plates with yeast paste containing 5 mM all-*trans*-retinal. Larvae were carefully transferred under low red light conditions to 2% agar plates with a 1 ml water film. CsChrimson was activated with 625 nm light (high: $8.13\mu\text{W}/\text{mm}^2$ or low: $1.13\mu\text{W}/\text{mm}^2$) for 5 s. Videos were taken during the experiment and analyzed using the Fiji cell counter plugin (ImageJ, NIH, Bethesda). Rolling was defined as at least one complete 360° roll along the body axis. Bending was defined as a c-shape like twitching, typically seen before rolling behavior, and not to be confused with other described bending behavior.¹⁵ Turning behavior describes head turning and thereby a direction changes of locomotion. Backward behavior describes at least one wave of backward crawling. Stop behavior describes a stop of locomotion. Hunch behavior describes a full body contraction. No behavior describes the absence of a change in larval behavior. Staging, behavioral assays and analyses were performed in a blinded and randomized fashion.

Calcium imaging in intact larvae

Calcium responses were recorded from the soma of specific neurons labeled with $UAS-GCaMP(6\text{ s or }7\text{ s})$ or $UAS-jRCaMP1b$ under the control of specific neuronal Gal4-drivers ($v'td2: 73B01-Gal4$; $v'td1/2: 35B01-Gal4$; $v'td2/Ca4\text{ da: }Gr28b.c-GAL4$; $Dp7: IIP7-Gal4$;

ABLK: *Lk-Gal4*, . Live third instar larvae (94 ± 2 h) were mounted in 90% glycerol and immobilized with a coverslip. The neuronal somata were live imaged by confocal microscopy with a 40x/NA1.3 oil objective (Zeiss LSM700 or LSM900AS2). 400 frame time series were acquired at a frame rate of 0.24 s or 0.34 s (240×240 pixels) and the larva was subjected to UV light for 10 s (365–525 nm, 10–60 $\mu\text{W}/\text{mm}^2$ CoolLED). Each larva was subjected to at least 2 pulses of UV light during the 400 frame time series with an interval of at least 15 s between pulses. For each genotype, 5–10 larvae were assayed between ZT 3 to 6. Calcium imaging was performed with identical confocal microscope settings imaging a single plane (approx. 2 μm thickness). Only datasets without significant Z-drift (stable baseline, return to original baseline levels after stimulation) were retained for analysis.

Optogenetic activation of C4 da (*27H06-LexA*), BO (*GMR-LexA*) or Dp7 (*Ilp7-LexA*) neurons with CsChrimson (*LexAop-CsChrimson*), or inhibition/ablation (C4 da/Dp7: *LexAop-TnT*, BO: *GMR-hid*) and calcium imaging in ABLK neurons (*Lk-Gal4*, *UAS-GCaMP6s*), were also performed in intact 3rd instar larvae. For optogenetic activation experiments, animals were reared in grape agar plates supplemented with all-trans retinal in the dark. Imaging was performed under low light conditions. Larvae were mounted and imaged as described above. A red light pulse for CsChrimson activation (635nm, intensity: 700 $\mu\text{W}/\text{mm}^2$) or UV light pulse for native stimulation (365 nm, 60 $\mu\text{W}/\text{mm}^2$) was given using an optical fiber-coupled to CoolLED Pe4000 light source. For each genotype, 5 larvae were assayed with identical confocal settings.

To visualize NPPR^{Ilp7} release, we imaged either Dp7 soma or lateral dendrite (*Ilp7-Gal4*, *UAS-NPPR^{Ilp7}*) that features NPPR^{Ilp7} puncta as well as synaptic input and output of v^{td2} and ABLK neurons, respectively. Time series with 500 frames were acquired at 0.24 s/frame (Zeiss LSM700).

Calcium imaging in semi-intact larvae

For comparison of noxious light versus mechanonociception, ABLK neuron calcium responses were assayed in semi-intact larval preparations essentially as described.³⁰ Staged 94 ± 2 h old larvae were partially dissected on a Sylgard (Dow Corning) plate in physiological saline³⁷ (120 mM NaCl, 3 mM KCl, 1.5 mM CaCl_2 , 4 mM MgCl_2 , 10 mM NaH_2CO_3 , 10 mM Glucose, 10 mM Trehalose, 10 mM Sucrose, 5 mM TES, 10 mM HEPES). ABLK neuron somata expressing GCaMP6m were imaged by confocal microscopy with a 40x/NA 1.0 water objective (Olympus FV1000MP). A micromanipulator-mounted *von Frey* filament (45 mN) was used to provide a mechanonociceptive stimulus to midabdominal segments (A3–A5). For noxious light stimulation, the larval preparation was subjected to UV light for 10 s (365 nm, 60 $\mu\text{W}/\text{mm}^2$ CoolLED).

Cell culture and co-immunoprecipitation assay

Biochemical interaction of Lgr4 and Ilp7 in S2 cells was assayed by transient co-transfection using a previously established protocol.¹¹⁶ For S2 cell expression the following constructs were used: pUAST-AttB-Lgr4-3xflag-6xHis (wildtype, I264A and ΔLRR variants), pUAST-AttB-Ilp7-HA, pActin-Gal4. Cells were seeded in 6 well plates and transfected at 50% density in an adherent state using Effectene (QIAGEN, Venlo, Netherlands). Cells were harvested 48 h post-transfection and lysed in 500 μL lysis buffer (50 mM Tris pH7.4, 150 mM NaCl, 1% Triton X-100, protease inhibitor mix (Roche)) for 20 min on ice. After centrifugation (10 min/4°C/10,000 \times g), the supernatant was incubated with mouse IgG-agarose (Sigma-Aldrich, St. Louis, MO) for 30 min at 4°C, and subsequently with anti-flag M2 agarose beads (Sigma-Aldrich, St. Louis, MO) or anti-HA Sepharose beads (Roche) for 4 h at 4°C. Samples were washed with lysis buffer three times, denatured and analyzed on Bis-Tris gels (ThermoFischer) and by western blotting against Ilp7-HA (rat anti-HA, 1:5000, Roche) and Lgr4-3xflag (anti-flag M2, 1:10,000, Sigma). Experiments were repeated three times.

qRT-PCR

The material used for each qRT-PCR sample ($n = 3$ per genotype) was obtained from 5 synchronized L3 males 94–96 h after egg-laying for 2 h in apple plates. 48 h after the egg laying, 30 larvae were transferred from the apple plates into a vial with fly food to avoid competition. The genotypes used were *y[1] w[*] Mi{Trojan-GAL4.1}Lgr4[MI06794-TG4.1]* or *P{w[+mW.hs] = GawB}109C1, y[1] w[*]*, which served as a *yw* background control for the *Lgr4* TROJAN insertion. Male larvae were selected under the stereoscope and immediately put into dry ice and either stored in -80°C or processed for RNA extraction immediately. Each sample was macerated using pellet pestles, homogenized in 800 μL TriPure Isolation Reagent (Roche), and centrifuged at 12000 g for 1 min, to remove tissue debris. We added 0.5 volume of absolute ethanol (400 μL) to the supernatant and then followed manufacturer's instructions from the kit High Pure RNA Tissue Kit (Roche). An extra DNase treatment (Turbo DNA-free kit, Ambion, Life Technologies) was performed to reduce gDNA contamination. 1 μg of RNA was used for the cDNA synthesis using the Maxima First Strand cDNA Synthesis Kit for RT-quantitative PCR (Thermo Scientific), following manufacturer's instructions but for a final volume of 10 μL .

qRT-PCR primers were designed and their specificity tested using Primer BLAST or Primer3. Primer efficiencies were determined to be between 90%–100% using qPCR standard curves using serial dilutions (1x, 0.1x, and 0.01x) of gDNA extracted from the genome reference stock #2057 (BDSC) extracted using the High Pure PCR template preparation kit (Roche). The resulting melting curves did not present primer dimers in any concentration or in water.

Briefly, the experiments were performed in a Lightcycler 96 (Roche) using the FastStart Essential DNA Green Master dye and polymerase (Roche). The final volume for each reaction was 10 μL , consisting of 5 μL of dye and polymerase (master mix), 2 μL of 10 \times diluted cDNA sample and 3 μL of the specific primer pairs (1 μM each). qRT-PCR primers used are listed in Table S2.

Light avoidance pupariation assay

w¹¹¹⁸ and *Ilp7^{ko}* flies (3–6-days-old) were crossed and after 1–2 days transferred to laying pots with grape juice agar plates for 48 h. The next morning, the animals were allowed to lay eggs in fresh plates with yeast within a fixed time-frame (Zeitgeber (ZT) 4–6) for 1–2 h depending on the number of fertilized eggs to minimize the risk of overcrowding (the first plate was discarded). 3rd instar foraging larvae (94 h ± 1.5 h AEL) were then collected and placed in a tube containing standard medium. This tube was mounted in a T-shape glass device designed as described previously,³⁶ where half of the horizontal glass tube is covered by black electrical tape. This allows larvae to wander and pupariate either in the dark or in the light side. Larvae were kept for 3 days under constant white light (2.9–4.5 μW/mm²) at 25°C. The numbers of pupae in both dark and light sides were then counted. The Preference Index (PI) was calculated as: (number of puparia in dark- number of puparia in light)/total number of puparia.

Developmental time assay

w¹¹¹⁸ and *Ilp7^{ko}* flies (2–9 days old) were crossed and maintained at 25°C in laying pots with grape juice agar plates for 48 h. Flies were then transferred to a fresh plate to lay eggs for 1–2 h. To control for overcrowding, 20–30 2nd instar larvae (48 h AEL) were transferred to vials containing normal *Drosophila* food at 25°C. The number and timing of pupariation was assessed 3 times/day every 6–8 h until all larvae pupariated or died. Pupariation was defined as cessation of movement with evaginated spiracles and a darker color of the puparium.

QUANTIFICATION AND STATISTICAL ANALYSIS

Statistics

Sample sizes were chosen similar to previous publications and commonly used in the field.^{14,15,30,48,113} For comparison of two groups, unpaired Student's t test with Welch's correction was used, or nonparametric Mann-Whitney U test in case of non-normal distribution of the data. For analysis of mechanonociceptive behavior, the χ^2 test was used. For multiple comparisons, one-way ANOVA with Tukey's post hoc analysis was performed. All tests were two-tailed and differences were considered significant for $p < 0.05$ (* $p < 0.05$, ** $p < 0.01$, *** $p < 0.001$, **** $p < 0.0001$). Statistical testing was performed using Prism (GraphPad). Exact P values for all quantitative data comparisons are listed in [Table S1](#).

Analysis of network synaptic counts

Network graphs were built by using the customized graph tools on CATMAID, where the interactions between a pair of nodes (neurons) was generated based on the absolute number of synaptic counts, using a synapse cutoff above 2¹⁴. The network was built starting with the first processing layer (sensory neurons) consisting of 3 nodes, each representing a subset of sensory neurons (C4 da, v'td1 and v'td2) connected to Dp7 neurons (second processing layer). Intermediate nodes from the sensory neurons to Dp7 were also extracted. The third processing layer consisted of output nodes of Dp7 neurons with a) VNC projections and b) being interconnected with sensory neurons (Hugin-VNC and ABLK). The thickness of the arrow between 2 nodes was determined automatically in CATMAID as a function of synaptic counts. Analysis of synaptic counts between different neurons connected on the lateral Dp7 domain was done using Graph Pad Prism (GraphPad, San Diego, CA, USA).

Developmental toxicity assay

Bar charts displaying percentages of animals were plotted with Excel, whiskers depict standard deviation. Statistical significance was calculated using the χ^2 test (GraphPad, San Diego, CA, USA).

Light avoidance analysis

Preference index (PI) was calculated at 15 mins as: (number of larvae in dark-number of larvae in light)/total number of larvae. PI data are shown as violin plots, where the middle line shows the median. If more than 3 larvae escaped during the trial, it was discarded. Statistical analysis was performed using one-way ANOVA and Tukey's post hoc test (GraphPad, San Diego, CA, USA).

Analysis of temporal larval distribution was performed by keeping only every 200th frame, cropping and converting mp4 files to avi using a custom script and ffmpeg (<https://www.ffmpeg.org>). Reduced avi files were processed and analyzed in Fiji (ImageJ, NIH) using a custom macro script to create background-corrected masked images retaining intensity-based signals from larvae only. Total intensities on the dark and light side were measured over time and plotted as a preference index (PI = (intensity in dark- intensity in light)/total intensity) analogously to larval distribution. All scripts and code used are available at https://github.com/formozov/larva_tracking_lmambocus_et_al.

Mechanonociception analyses

Statistical significance was calculated using the χ^2 test (GraphPad, San Diego, CA, USA).

Locomotion and chemotaxis analysis

For locomotion analysis, velocity and bending angles were analyzed using the FIMTrack software (<https://github.com/kostasli/FIMTrack>). For analysis, only animals displaying continuous locomotion and uninterrupted tracking were kept. Other animals were excluded from analysis. Average locomotion speed and cumulative bending angles were analyzed and plotted for the first 30 s under

dark or blue light conditions. Graphs of mean \pm s.d. were plotted and analyzed using one-way ANOVA and Tukey's post hoc test (GraphPad, San Diego, CA, USA).

For chemotaxis, the locomotion tracks were generated using the FIMTrack software. All reconstructed tracks were considered in the analysis. The plate was virtually divided into four equidistant regions along x axis. The first and the last regions were further restricted along the y axis (to take only a central band with a width equal to the radius of the plate) to set a "no-odor" and "odor" zone, respectively. The area surrounding the odor was defined as the "odor" zone, while the same area on the opposite side of the plate was defined as the "no-odor" zone. To quantify chemotaxis we used a performance index (PI), defined as $(t_{\text{odor}} - t_{\text{noodor}}) / (t_{\text{odor}} + t_{\text{noodor}})$, where t_{odor} and t_{noodor} are total time that larvae spent in the odor and no-odor zones, respectively, in the time window between 3 and 5 min of a given video recording. Graphs of mean \pm s.d. were plotted and analyzed using one-way ANOVA and Tukey's post hoc test (GraphPad, San Diego, CA, USA).

Analysis of calcium imaging

Time series analysis was performed using image registration with the StackReg plugin (using translation function, Fiji, ImageJ) to correct for internal movement. GCaMP6 signal intensity was then quantified using a region of interest defining the neuronal soma and the Time Series Analyzer V3 plugin (Fiji, ImageJ). The calcium response ($\Delta F/F_0$ (%)) was calculated by subtracting the amplitude of pre-stimulation baseline (average of 19 frames) from the stimulation evoked amplitude. $\Delta F/F_0$ (%) = $(F - F_0)/F_0 \times 100$. Maximum fluorescence was calculated as $F_{\text{max}} - F_0/F_0 \times 100$ (F_{max} , maximum fluorescence observed during the stimulation; F_0 (average of 19 frames)). Graphs of mean \pm s.e.m were plotted using Prism (GraphPad, San Diego, CA, USA). Comparison of maximum responses ($\Delta F_{\text{max}}/F_0$ (%)) were plotted as boxplots (box showing median and 25th and 75th percentile, whiskers 1st and 99th percentile), and analyzed using one-way ANOVA and Tukey's post hoc test (GraphPad, San Diego, CA, USA).

Analysis for calcium imaging data upon optogenetic activation of C4 da, BO and Dp7 neurons were performed as described above.

To analyze NPPR^{lpp7} release, the baseline signal was calculated from 19 frames before 40 frames of UV illumination, with 100 frames between stimulations. NPPR^{lpp7} release events were calculated for each puncta using the formula $\Delta F/F_0$ (%) = $(F - F_0)/F_0 \times 100$. The n number refers to individual LDCV puncta from 5 different larvae.

For calcium responses in semi-intact larval preparations, baseline (F_0) and the relative maximum intensity change (ΔF_{max}) of GCaMP6m fluorescence was analyzed. $\Delta F_{\text{max}}/F_0$ values of mechanonociceptive versus noxious light ABLK neuron responses were plotted and compared, with the centerline representing median values, upper and lower whiskers representing SEM. Statistical significance was analyzed using a Mann-Whitney U test. Analysis of Somatic Dp7 calcium responses upon optogenetic activation of v^{td2} neurons was performed described above. Comparison of maximum responses ($\Delta F_{\text{max}}/F_0$ (%)) were plotted as boxplots (box showing median and 25th and 75th percentile, whiskers 1st and 99th percentile) and analyzed with the Mann-Whitney U test.